



Progress in flexible dye solar cell materials, processes and devices

| | |
|-------------------------------|---|
| Journal: | <i>Journal of Materials Chemistry A</i> |
| Manuscript ID: | TA-FEA-02-2014-000902.R1 |
| Article Type: | Feature Article |
| Date Submitted by the Author: | 09-Apr-2014 |
| Complete List of Authors: | Brown, Thomas; University of Rome Tor Vergata, Dept. Electronic Engineering De Rossi, Francesca; University of Rome Tor Vergata, Dept. Electronic Engineering Di Giacomo, Francesco; University of Rome Tor Vergata, Dept. Electronic Engineering; University of Rome Tor Vergata, Electronic Engineering Mincuzzi, Girolamo; University of Rome Tor Vergata, Dept. Electronic Engineering; University of Rome Tor Vergata, Electronic Engineering Zardetto, Valerio; University of Rome Tor Vergata, Dept. Electronic Engineering; University of Rome Tor Vergata, Electronic Engineering Reale, Andrea; University of Rome Tor Vergata, Dept. Electronic Engineering; University of Rome Tor Vergata, Dept. Electronic Engineering Di Carlo, Aldo; University of Rome Tor Vergata, Dept. Electronic Engineering; University of Rome Tor Vergata, Dept. Electronic Engineering |
| | |

Progress in flexible dye solar cell materials, processes and devices

T. M. Brown^{*a}, *F. De Rossi*^a, *F. Di Giacomo*^a, *G. Mincuzzi*^a, *V. Zardetto*^{a,b}, *A. Reale*^a, *A. Di Carlo*^a,

^a *C.H.O.S.E. (Centre for Hybrid and Organic Solar Energy), Department of Electronic Engineering, University of Rome - Tor Vergata, via del Politecnico 1, 00133, Rome, Italy*
^b *Department of Applied Physics, Eindhoven University of Technology, P.O. Box 513, 5600 MB Eindhoven, The Netherlands*

*E-mail: thomas.brown@uniroma2.it

Abstract

Flexible Dye Solar Cells (FDSCs), in their most widespread architecture, are assembled with two opposing planar film or foil substrates in metal/plastic or plastic/plastic combinations. The use of one metal electrode enables the convenient utilization of materials and high temperature processes but is accompanied by issues including partial opacity of the electrolyte and catalyst layer. Constraints on the stability of plastic substrates has led to the development of a variety of alternative material formulations and processes to guarantee performance even at low temperatures compatible with plastic films. Recently, efforts in doing without transparent conducting oxides have led to the development of new unconventional architectures. Review of the operation of DSCs shows that initial target markets are represented by indoor applications where power outputs densities have been shown to outperform some of the main

competing flexible photovoltaic technologies. Whereas performance, stability in particular, needs to be significantly improved for the adoption in long term outdoor installations, commercial products integrating FDSCs for indoor or portable use have already been launched. Issues pertaining progress in materials, processes, devices and industrialization of FDSCs will be analyzed and discussed in this review.

1. Introduction

Dye Solar Cells (DSCs)¹⁻³ represent an attractive photovoltaic technology, initially developed on glass substrates, which has seen growing efforts and success in its application to flexible substrates. Glass provides an extremely effective barrier towards water and oxygen penetration into the device and enables the utilization of high-temperature processes (when coated with fluorine-doped tin oxide, FTO, rather than indium tin oxide, ITO) for the fabrication of efficient DSCs and is well suited for building integrated photovoltaics (PV). Nevertheless, the drawbacks of this type of substrates consist mainly in their rigidity, weight, and fragility which limit the potential integration of DSC devices in portable electronics and their conformability to any surface, even curved ones.

Based upon these considerations, alternative, low-cost, lightweight, and flexible substrates, such as plastic films and thin metal foils, have been investigated for the fabrication of DSC electrodes. The development of flexible dye solar cells (FDSCs)⁴⁻⁸ not only addresses the needs of applications where portability, conformability, reduced dimensions and weight are important, but is also conducive to industrial roll-to-roll (R2R) fabrication which enables the implementation of high throughput production lines and its associated potential reduction in manufacturing costs.

Here we will review recent progress in flexible DSCs. After a short run through the basic device structure and operation (section 1), the first section on the materials utilized and developed for FDSCs will focus on the foundations on which the devices are developed: i.e. the substrates (section 2). These, represent a tremendous opportunity for both manufacturing and applications, but also set important constraints on materials and especially processes which can be applied to manufacturing. Since at least one of the two substrates comprising the FDSC has to be made out of transparent plastics, processing temperatures have to be typically kept lower than 120-150 °C. Whereas those utilized for glass DSCs are typically higher than 400 °C (for the conventional sintering of the TiO₂ layer and the conversion of catalyst precursors), researchers have innovated and developed alternative materials, deposition and post-processing techniques with which to

assemble the devices on flexible substrates, which, at the state of the art, deliver not only uncompromising output power densities but also carry commercial appeal especially for the application in specific environments. As we will see, plastic substrates also impact FDSC technology because of their high gas permeation rates which can limit their lifetime. In fact, encapsulation strategies are discussed in section 9 after sections dedicated to photoelectrodes (PE, section 4), counterelectrodes (CE, section 5), dyes (section 6), electrolytes (section 7), large area modules and their fabrication (section 8), and encapsulation and lifetime (section 9). The operation, applications, costs and markets for FDSCs will be discussed in section 10, new architectures and concepts in section 11 before finishing with the conclusions and outlook of this review.

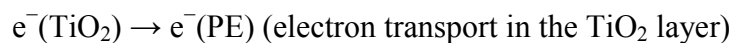
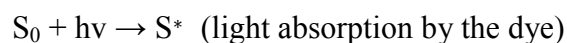
2. Basic structure and operation

Figure 1 shows the basic operation of a DSC^{2, 3, 9-11} in its simplest form, i.e. that of two conducting substrates which sandwich the active materials. The photons are absorbed by dye molecules, which are anchored to (and cover) a mesoporous, high-surface-area layer (to maximize dye uptake and thus light absorption) of a nanocrystalline high band gap semiconductor (typically TiO₂) with a consequent excitation of electrons from the low energy state to a high energy state of the dye. The exciton is split at the TiO₂/dye interface due to the energy difference and

proximity in wavefunction density between the lowest unoccupied molecular orbitals (LUMO) of the dye and the conduction band of the TiO₂ in which the electrons are injected. Here the electrons diffuse through the TiO₂ film, are collected at the transparent conducting oxide, TCO, and driven through the external circuit. The oxidized dye molecules are regenerated back to their neutral state by the electrons provided by the iodide (I⁻) species in the electrolyte which are converted in triiodide (I₃⁻). The build-up of I₃⁻ at the photoelectrode creates a concentration gradient so that the ions diffuse to the counterelectrode where their reduction back to I⁻ is catalyzed by a catalyst layer¹⁰.

The main reactions giving rise to the photovoltaic effect can be summarized as:

Electron-collecting Photoelectrode (PE)

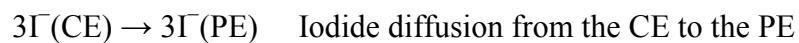


Counterelectrode (CE)



material, Pt in figure 1)

Electrolyte





The above reactions compete with recombination of photoexcited electronic charge, mainly those in the TiO_2 and the conducting electrode with either holes in the oxidized dye or more significantly with the red-ox species in the electrolyte. At low light intensities the electrode-electrolyte recombination path becomes the dominant route for the back transfer of electrons to tri-iodide, reducing the photovoltage of the DSC. It can be limited by thin compact layers over the photoelectrode arising (naturally or induced) on titanium foils or by inserting specific thin films between the electrode and the mesoporous TiO_2 layer¹². In depth reviews of the operation and dynamics of DSCs can be found in references 2, 3, 9-11, 13, 14.

Figure 1 represents the flat sandwich-type architecture most commonly utilized for cells where both substrates are transparent: i.e. glass/glass for rigid devices or plastic/plastic for flexible devices. FDSCs of this type come in three different configurations according to whether metal or plastic are used as electrodes (see Fig. 2). Metals can withstand high temperatures so that material formulations and processes developed for glass DSC technology can be readily applied. Typically it is the photoelectrode which is metallic (Fig. 2a) since it permits high temperature sintering of the mesoporous TiO_2 layer which has a strong bearing on device efficiency because temperatures of 450-500 °C guarantee an optimal degree of

electromechanical bonding between the nanoparticles (and these to the conducting substrate) and thus sufficiently long electron lifetimes for effective charge collection.^{15, 16} The counterelectrode¹⁷⁻¹⁹ then has to be transparent and is made of TCO/plastic coated with a catalytic layer deposited with compatible techniques. Although this metal PE configuration has the advantage of maximizing photoelectrode performance, light has to pass through the CE and tens of microns of electrolyte solution where a significant fraction of photons are absorbed before reaching the active dye molecules. Because of this, CE- (or back-) illuminated cells yield photocurrents which can be as much as 30% - 40% lower compared to the same transparent cells illuminated through the PE^{20, 21} unless more transparent electrolytes are formulated. Thus, the other main configuration for FDSCs utilizes all plastic electrodes (Fig.2b) so that light can be shone directly through the PE. The challenge in this latter case is to develop TiO₂ films at low temperatures (< 150 °C) which are as effective in collecting charge as their counterparts processed at high temperatures.

3. Substrates

Second generation thin-film solar cells, due to the relatively high temperatures reached, have been realized preferably either on high glass transition temperature polyimide plastic films or on stainless steel substrates. Power conversion

efficiencies of 12.5-16.3% have been reported in triple junction amorphous silicon devices on polyimide,²² 13.6% in CdTe on metal,²³ and 20.4% in CIGS on polyimide.²⁴ Instead, for flexible dye solar cells, the more transparent and lower cost polyethylene terephthalate (PET) and polyethylene naphthalate (PEN) polymers have represented the most common substrate choice. They act as widely-used transparent conductive substrates electrodes when coated with ITO.²⁵ The sheet resistance of ITO/polymer substrates reaches 10-15 Ω/\square , close to the typical value of FTO-coated glass (7-15 Ω/\square) maintaining high transparency in the visible spectrum, with costs which are similar or in the same range.⁷ Notwithstanding its good transparency/conductivity properties, ITO on plastic has a number of issues. Firstly, ITO is a brittle material, sensitive to tensile and compressive stress (e.g. during bending) leading to conductivity degradation. In addition damage greatly depends on the thickness of ITO layer and the substrate itself. In particular for high conductivity ITO (15 Ω/\square), a previous study shows that curving devices with radii above 14 mm no degradation effects occur but crack formation and propagation does appear for lower radii.²⁶ Secondly, despite ITO-coated substrates provide good resistance towards the solvents typically used in DSC fabrication,²⁶ its stability in the electrolyte solution is not always guaranteed and can vary greatly according to the additives used in electrolyte composition^{27, 28} (see section 7). Different materials such as graphene,²⁹ **Error!**

Reference source not found.carbon nanotubes,³⁰**Error! Reference source not found.** and conductive polymers,³¹ **Error! Reference source not found.**have been investigated to replace ITO due to the drawbacks accompanying this coating³². The main limit of these conductive PET and PEN substrates consists in their maximum practical processing temperatures of around 150 °C.²⁶ In fact ITO-polymer substrates start to deform with temperatures above that range, and even melt at 235 °C.²⁶ High thermally-resistant films such as clays, and polyimides have been investigated as substrates to overcome the 150 °C barrier. However since their transparency is low, CE-rear-side illumination is required which leads to device efficiencies which are lower compared to those assembled with PET and PEN.^{33, 34} Finally plastic films are very sensitive to water and oxygen permeation with a water vapour transmission rate (WVTR) of 1-10 g m⁻² day⁻¹, which is ~ 6 orders of magnitude higher than the common target range of 10⁻⁶ gr/m²/day which can be comfortably sustained by glass.^{35, 36} The stability of FDSCs can be compromised by permeation of oxygen and water molecules from the outside and their interaction with dye and charge mediators. Thus, the deposition of multilayer films (inorganic/organic or pure inorganic), acting as low permeation barriers, on the films' surfaces has been the most reliable approach to reduce WVTRs to 10⁻⁵-10⁻⁶ g m⁻² day⁻¹.³⁶ **Error! Reference source not found.** Different methods such as sputtering,³⁷ plasma enhanced or initiated chemical

vapor deposition,³⁸**Error! Reference source not found.**³⁹**Error! Reference source not found.** atomic layer deposition,^{35, 40}**Error! Reference source not found.** and strategies such as multilayers,^{41, 42}**Error! Reference source not found.** have been successfully implemented for lowering permeation rates and tested in other optoelectronic technologies such as organic light emitting diodes (OLEDs) and photovoltaics (OPV) but systematic investigations need to be carried out in FDSCs.

Thin metal foils^{4, 7} can be valid alternatives to conducting plastic films, since they withstand the high temperatures required during conventional effective manufacturing processes. Furthermore they provide excellent conductivity compared to TCOs and a better barrier to moisture or oxygen ingress. However, when fabricating large-area series-connected modules, metal foils (unless used only as carriers) need to be cut into individual cells in order to guarantee electrical isolation whereas for plastic substrates scribing of the TCO is sufficient. Since metals are opaque, the other substrate used for completing a DSC must be transparent to allow light to penetrate into the device where it is absorbed by the dye molecules. The key requirement for a metal electrode foil in a liquid-based DSC is the chemical inertness towards the corrosive electrolyte. Different metals have been investigated such as aluminum, copper, iron, nickel, zinc, stainless steel (StSt), titanium (Ti), and alloys such as Inconel.^{4, 43-47} Simple soaking tests

revealed that only some types of StSt, Ti and Inconel are stable and thus suitable for the fabrication of DSCs. However the stability of the last three metals seems to be different depending on whether they work as PEs or CEs. Miettunen et al. have studied StSt, Ti and Inconel in both the configurations, highlighting large differences in corrosion behavior,^{44, 48} which is well known to be function of the voltage applied to the electrode.⁴⁹

Among these metals, high purity (> 99%) titanium foils are the most stable and resistant to corrosion due to a natural passivating oxide forming on its surface. The drawback of this material is the higher cost (12-40 \$/m²) compared to StSt sheets (4 \$/m²).⁷ Other cheaper metals such as stainless steel (StSt), nickel or aluminium may be made to work as well if properly protected from the electrolyte, e.g. by TiN/polyimide composite coatings on the photoelectrode⁵⁰ or by sufficiently thick catalyst overcoats on the counterelectrode⁵¹.

Recently metal meshes, also developed for OLEDs and OPV⁵², composed of very thin metal wires (StSt or Ti) have been successfully integrated in new types of TCO-free FDSC architectures which are particularly appropriate for applications where strong flexing is desirable, yielding also high power conversion efficiencies (PCEs of over 6%).⁵³ Metal meshes⁵⁴ can be less expensive than foils (Ti meshes 15–20 \$/m², StSt meshes 0.1 - 0.25 \$/m²),⁷ and are also transparent thus overcoming the drawback of having to illuminate through the CEs. The most

suitable aperture/distance between two wires has been shown to be different whether metal meshes were developed for PEs or CEs. For PEs it was around 15-20 microns, **Error! Reference source not found.** similar to the diffusion length for electrons in the TiO₂ layer so as to ensure efficient charge collection.^{55, 56} For CEs the aperture size could be increased up to millimeters according to Xiao et al.⁵⁷

4. Photoelectrodes

The most utilized material for the fabrication of the electron-collecting photoelectrode is a mesoporous nano-crystalline TiO₂ (nc-TiO₂) deposited in one or more layers over the conducting substrate with thicknesses ranging from a few microns up to around 15 microns depending on the dye and charge mediator combinations. It possesses the right properties in terms of energy levels and electron mobility, especially in its anatase state.⁵⁸ TiO₂ is a large band gap n-type semiconductor with an energy gap of 3.2 eV (absorbing only in the UV). Absorption of the visible solar spectrum is through a dye anchored to the TiO₂ which, due to the high surface area of the mesoscopic film (around three orders of magnitude larger than a flat surface⁵⁹), guarantees photoexcitation of a large number of molecules and high photocurrents. The conduction band lies a few hundred meV under the LUMO of the dyes, allowing for efficient charge

injection.² The TiO₂ requires a sintering step after deposition to obtain the right porosity/surface-area (for dye loading) and sufficient electromechanical bonding between nanoparticles to achieve sufficiently long electron lifetimes, effective transport and collection at the electrode. Lowering the concentration of defect and traps states is accompanied by lower recombination rates and thus higher diffusion lengths.⁶⁰ Attention should be addressed to the deposition and processing technique, which will influence morphology of the PE. Moreover, to obtain a truly flexible DSC, the TiO₂ layer should resist to the stresses generated by bending the device.

The fabrication of TiO₂ photoelectrodes can be divided into four steps: synthesis, and dispersion of TiO₂ nanoparticles into coatable or printable pastes, deposition on the conducting substrate and post-processing of the layer. Additionally, pre-treatment of the nanoparticles and/or the substrate has been implemented in a number of works. TiO₂ synthesis can be avoided by purchasing commercial TiO₂ particles or ready-made printable dispersions/pastes. For glass-based DSCs, the common procedure to prepare the photoelectrode consists in dispersing the nanoparticles together with a (cellulose) binder to formulate a paste, screen printing and firing the paste at 450-500 °C to remove the binder and sinter the nanoparticles together to form a mesoporous structure before dye sensitization.⁶¹ Alternative approaches for fabricating the TiO₂ layer, such as sol-gel synthesis

with templating agents, are also present in the literature.⁶²⁻⁶⁵ Nevertheless, for devices with substrates that can withstand them, application of high temperatures represents the most common treatment to guarantee the required sintering quality. Instead, especially for plastic substrates, alternative material formulations and processes have been developed for the PEs.

4.1. Photoelectrodes on plastic substrates

When the photoelectrode is prepared on ITO-coated plastic substrates (Table 1), the set of possible processes available are constrained by the lower chemical stability of ITO respect to FTO^{66, 67} and especially by the maximum processing temperatures that can be utilized (~150 °C) which also limit the effectiveness of the PEs if the typical TiO₂ paste formulations are utilized,⁶⁸. To reach levels of uncompromising performance, scientists have thus developed a range of material formulations and processes which are different from the standard ones used for glass-based devices.

4.1.1. TiO₂ and wide band gap photoelectrode materials

Nanocrystalline films of TiO₂ are the most popular and currently the best-performing photoelectrode structures. The most-used approach consists in preparing a binder-free paste (made of nanoparticles, solvents such as alcohols and/or water and additives with low boiling points but no binders which are useful

for their film-forming properties but do not decompose off at the low temperatures compatible with plastics), coating it on the ITO substrate and heating it up to 150°C to remove solvents and additives and promote slight sintering.⁶⁹ Further or alternative post-processing techniques have been developed as will be detailed below. Nanoparticles can be synthesized in the laboratory or commercially sourced. For the latter kind, Degussa P25 powder is widely utilized. These particles are cubic with rounded edges with a mean diameter of ~20 nm and a BET area of 55 m² g⁻¹.⁷⁰ The production of P25 is performed using the AEROSIL© process allowing production in very high-volumes.⁷¹ The maximum published PCE obtained with this powder in a plastic-based FDSC (sensitized by a single dye) is 6.3%,⁷² whereas PCEs above 8% were obtained using hydrothermally custom-synthesized TiO₂ nanoparticles.^{73, 74} The most efficient plastic DSCs amongst these were realized by mixing together different particles with diameters of 20 and 100 nm in order to obtain high surface areas and efficient transport through the mesoporous structure. In fact adding even very small (d < 5 nm) TiO₂ particles promotes necking between these⁷⁵⁻⁷⁷. The same strategy of mixing different diameters has also been implemented utilizing commercial particles yielding devices with a PCE of 6.5%.⁷⁸ The concept of adding materials to promote necking between particles at low or even room temperatures, sometimes referred to as nanoglues, has been an effective route for

PE fabrication^{76, 79} aiding not only the efficiency of FDSCs with low-T PEs (a PCE of 5.43% was achieved in films containing the TiO₂ interparticle binding agent synthesized by a sol-gel process)⁷⁹ but also mechanical flexibility.

A recently developed alternative approach (see Fig.3, left) consisted in preparing much larger submicron- to micron-sized “building blocks” (such as prefabricated mesoporous TiO₂ beads), by using solvothermal synthesis or by sintering nanoparticles into clusters (even at high temperatures before their deposition).⁸⁰⁻⁸³

In this way it was possible to obtain strongly interconnected TiO₂ networks while maintaining the advantage of solution-processing of the TiO₂ layer, delivering devices with PCEs of 7.5%.⁸³ The blocks can be physically and chemically treated prior to integration on the photoelectrode. Pre-sintered P25 mesobeads have been treated with TiCl₄ (which is known to increase photocurrents in FTO/glass devices but damages ITO)⁸⁴ and then deposited with a cold vacuum spraying technique, without having to apply further processing steps such as heating, compression or UV.⁸⁵ Not only TiO₂ nanoparticles but also high aspect ratio pre-sintered TiO₂ nanowires have been successfully employed by transfer on plastic and a FDSC with a PCE of 5.5% obtained.⁸⁶

Recently, composites were used to improve the transport and/or flexing characteristics of the TiO₂ layer. TiO₂-coated double-walled carbon nanotubes were added to TiO₂ pastes to improve the electrical properties of the films

obtained at low temperatures, improving the PCE of the FDSCs from 3.0% to 3.9%.⁸⁷ TiO₂/polymers composites have been shown to improve cell bendability.⁸⁸ Polyvinylidene fluoride (PVDF) was successfully introduced in the mesoporous layer by simultaneously depositing TiO₂ by electrospraying and PVDF nanofibers by electrospinning (see Fig.4.⁸⁹). Subsequent compression at 80 MPa yielded devices with a PCE of 4.8%. The stresses of the fragile TiO₂ layer are transferred to the other component of the composite (the polymer fibres in that work) dramatically increasing bendability thus preventing delamination of the layer upon curving. Also (Sb,In)-doped SnO₂ (SITO) was used in FDSC photoanodes to enhance interconnection between P25 TiO₂ nanoparticles (see Fig. 5), not only raising the PCE from 4.5% to 6.8% but also its mechanical stability to bending.⁹⁰ HCl can also improve particle interconnection when added to a binder-free paste increasing device PCE from 4.0% to 5.0%.⁶⁶

Other materials have been used as alternatives to TiO₂ to fabricate flexible photoanodes including ZnO. The best ZnO-based FDSC (via electrophoretic deposition) showed a PCE of 4.0%.⁹¹ MgO-coated SnO₂ showed very high photocurrents (18 mA cm⁻²) with a PCE of 6.5%.⁹²

4.1.2. Deposition of the TiO₂ layers

In contrast to the TiO₂ pastes used for high temperature sintering on glass or metal foils which are commonly screen printed, most of the ones described above

relating to low-T TiO₂ on plastic substrates were deposited by the doctor blade technique because the absence of binders and additives in the TiO₂ paste makes screen printing difficult. As shown in Tables 1-2 doctor blade deposition is currently also the technique used to obtain amongst the highest PCEs both for plastic and metallic substrates.^{73, 74} Although optimization studies on the rheological properties of low-T TiO₂ pastes have been carried out (by adding an increasing quantity of ammonia or hydrochloric acid in water for example), the appropriateness of the doctor blade technique⁹³⁻⁹⁶ for large area (e.g. roll-to-roll) fabrication needs to be validated. Other techniques such as spin coating, gravure printing and ink jet printing have been used⁹⁷⁻⁹⁹ although PCEs under 5% are reported. Even if different sources mention low-temperature paste compositions for screen printing (the coating technique widely used for high temperature pastes on glass), which would be suitable for large area fabrication (as much as gravure printing for example), hardly any photovoltaic data have been reported.^{75, 100, 101} The only clear result reports a PCE of 0.25%.¹⁰² Cold vacuum spraying of pre-sintered P25 mesobeads was used to deposit a TiO₂ with no additional post deposition treatment. The resulting FDSC had a PCE of 4.2%.⁸²

Alternative techniques to printing include electrophoretic deposition (EPD). In EPD the flexible substrate is immersed in an electrically charged TiO₂ dispersion facing a conductive electrode. A voltage is applied between the substrate and the

electrode to deposit the mesoporous nc-TiO₂ layer or even multilayers of which the thicknesses can be easily fine-tuned. The best performing solar cell fabricated with EPD had a PCE of 6.6%.¹⁰³ A different route used to fabricate a strongly interconnected mesoporous TiO₂ layers consist in transferring on ITO/plastic films pre-sintered (at high-T) mesoporous TiO₂ previously made on glass or ceramic substrates.¹⁰⁴⁻¹⁰⁷ Adhesion of the transferred film on the plastic substrate was improved by depositing a thin TiO₂ adhesion layer prior to the transfer process. By using a double layer P25 photoanode with two different dyes a 6.6% PCE was obtained.¹⁰⁵

4.1.3. Post-processing of the photoelectrode

Since room- or low-temperature (120-150 °C) treatments do not typically guarantee sufficient necking between nanoparticles required to reach those maximum efficiencies achievable at high T,⁶⁸ apart from the introduction of necking agents (or nanoglues) in the paste formulations as outlined previously, other strategies consist in subjecting the deposited photoelectrodes to further processing such as compression, UV irradiation and chemical baths (compatible with plastic substrates) in order to improve device performance.

Static compression at 50-200 MPa was applied on the TiO₂ photoelectrode to obtain the first significantly efficient plastic FDSC with a PCE of 4.6%.¹⁰⁸ High pressure was applied during TiO₂ sintering to improve grain interconnection.¹⁰⁹

Continuous compression applied with a calender press (10 m/min), which may be particularly suited for R-2-R manufacturing, yielded almost the same performance as static compression, with PCEs equal to 4.7% and 5.1% respectively.⁹⁸ Although not yet applied to flexible DSCs it has been shown that utilization of both compression and temperature simultaneously (with a heated press) is beneficial⁶⁸. The most efficient plastic DSC (PCE of 8.1 %) was obtained applying 100 MPa of static compression on a mesoporous layer of hydrothermally synthesized nanoparticles.⁷⁴ UV-O₃ cleaning of the TiO₂ surface was used before dye immersion in order to improve its uptake. The effect of the applied pressure is shown in Figure 6. Using the same technique Fu et al. obtained a PCE of 7.0% using a photo-platinized CE.¹¹⁰

Compression is usually applied with an hydraulic press. However, a 200 MPa compression carried out with a cold isostatic press (CIP)^{96, 111} on a P25 TiO₂ film delivered a PCE of 6.3%⁹⁶. The P25 electrode became transparent after CIP compression, a transformation that has not been reported with hydraulic and calender presses. Compression is also used in the transfer technique to bond the high temperature sintered TiO₂ layer to the flexible substrate.¹⁰⁴⁻¹⁰⁷

Not only microwave irradiation has been utilized for sintering the TiO₂,^{112, 113} but also UV irradiation has been applied to TiO₂ films thanks to the latter's strong photocatalytical activity and capabilities to oxidize and remove organic

compounds.¹¹⁴ These characteristics were used to improve necking in the presence of a TiO₂ precursor, to remove organic additives present in the TiO₂ pastes and to clean TiO₂ surfaces before dyeing.^{74, 115, 116} A UV treatment (200 mW cm⁻¹) of a few tens of minutes, depending on layer thickness, completely removed the hydroxyl-ethylcellulose stabilizing binder in the TiO₂ film, led to a doubling of the PCE and better performance compared to equivalent FDSCs assembled with binder-free pastes.¹¹⁶ UV-irradiation is often coupled with other sintering procedures to optimize the final results. It was used together with SITO interconnecting agent to improve solar cell performance. The UV treated photoelectrode underwent a 100 °C water bath before the dyeing process. The use of the SITO nanoglue (Fig. 5), together with UV and water treatment led to a PCE of 6.8%, the highest value reported for a fully plastic DSC fabricated without compression.⁹⁰

UV scanning laser systems can represent an alternative to halogen lamps since they are highly automated, precise and selective¹¹⁷. They have been successfully implemented for sintering TiO₂ films leading to the same performance as oven sintering in glass DSCs.¹¹⁸⁻¹²⁰ Lasers have also been applied to flexible substrates¹²¹. Application of laser processing over flexible substrates is a challenging step due to the high fluences of the beams. Nevertheless, in situ laser sintering has been shown to boost efficiency in FDSCs by as much as 80%.^{122, 123}

Kim et al.¹²⁴ reported a method to transfer a TiO₂ film from glass (where is had been previously sintered) to a plastic substrate via laser detachment The film was subsequently subjected to high pressures to improve adhesion and a PCE of 5.7% was obtained for a plastic FDSC.

Photoelectrodes have also been treated in hot water (attempting to simulate a more complicated hydrothermal treatment which can convert amorphous TiO₂ in crystalline forms) although the PCE of resulting device was not high (i.e. 2.5%).¹²⁵ Sol-gel precursors can be added to paste composition, but can also be used for a chemical bath at a later stage. A chemical bath in titanium butoxide solution was used to improve bonding of a transferred TiO₂ layer.¹⁰⁷ Chemical vapour deposition of a sol-gel precursor coupled with UV irradiation has been shown to improve particle interconnection¹²⁶ as also a chemical sintering post-treatment using titanium n-tetrabutoxide.¹²⁷

4.1.4. Compact layers

To improve adhesion of mesoporous TiO₂ on flexible substrates, and to minimize recombination between the electrolyte and the TCO, a thin compact layer of TiO₂ can be deposited on the TCO surface.¹²⁸ The recombination-blocking behaviour can considerably improve performance of the solar cell especially when illuminated at low light levels or when a solid hole transporting material (HTM) is used, i.e. in solid state DSCs.¹⁴ In SSDSCs HTMs such as the organic

semiconductors P3HT or Spiro-O-MeTAD substitute the electrolyte and a metallic contact is directly deposited (usually by evaporation) over the HTM. In SSDSCs a compact layer separating the TCO from coming into contact with the HTM, thus suppressing strong recombination, is crucial.^{129, 130} The assembly of a TiO₂ compact layer on plastic substrates is not straightforward, since TiO₂ of low crystallinity is usually obtained at low temperatures. Sputtering is a feasible technique which has allowed to deposit 10 nm of semicrystalline TiO₂, with an associated PCE increase of 29%.¹³¹ No data on low levels of illumination or solid state architecture was reported.

Atomic layer deposition (ALD) is a layer by layer deposition technique used to deposit an amorphous films of TiO₂ at low temperatures.¹³² Since amorphous films have low charge mobilities, thicknesses should be large enough to completely cover the TCO but not higher in order to prevent strong ohmic losses. The optimal thickness of such a TiO₂ layer in a solid state flexible solar cell with a P3HT HTM was equal to 16 nm, while both 13 nm and 20 nm resulted in poor performance.¹³³ Results on glass were equivalent to devices made with compact layers obtained by spray pyrolysis (which represents a state of the art method to deposit crystalline compact layers at high T). Applied to FDSCs, the ALD layer led to a PCE of 1.9% (2.2 % on glass).

The paucity in available low-cost, efficient low-T compact layers represents an issue for indoor applications or solid state architectures for plastic-PE dye solar cells. Recently, new techniques to obtain low temperature compact layers by solution processing have been developed for flexible hybrid organometallic halide perovskite solar cells.¹³⁴ PCEs up to 10.2% were achieved with compact layers obtained by depositing a nanoparticle dispersion sometimes mixed with a sol-gel precursor or graphene.¹³⁵⁻¹³⁷ These materials and techniques may be well-suited for testing on FDSCs.

4.2. Photoelectrodes on metal substrates

When the flexible DSC photoanode is fabricated on metal foil (Table 2), such as Ti or stainless steel (StS), sintering at high temperatures is allowed. Titanium presents a much better surface in terms of thermal processing, paste adhesion, recombination inhibition, conductivity and barrier properties if compared to plastic TCO-coated substrates.⁶⁹ It is very stable to corrosion and is in fact the current choice for mass production.¹³⁸ G24 Power/Konarka reported a PCE of 7.17% at 1 Sun for cell sizes 0.402 - 1.69 cm² certified by NREL.¹³⁹ The Ti surface can be subjected to mechanical polishing and chemical baths in order to optimize charge collection by varying the native oxide morphology and composition.

The best-performing solar cells utilize hydrothermally synthesized TiO_2 or commercial pastes. The most efficient FDSC on metal foil fabricated with commercially available particles, such as Degussa P25 ($d=21$ nm) and P90 ($d=13$ nm), was obtained by the electrophoretic deposition technique followed by 100 MPa compression and annealing at 350 °C.¹⁴⁰ The PCE obtained was higher (i.e. 6.5%) with P90 owing to the larger surface area with respect to P25. This procedure allowed to obtain high PCE values at lower temperatures compared to the customary 450 - 500 °C and without pretreatment of the Ti foil.

Indeed a pre-treatment of the substrate is often used to obtain high performance cells.¹⁴¹ First, mechanical polishing was carried out to remove the native oxide and any contaminant arising on the surface during the fabrication of the foil raising the PCE of titanium FDSCs from 2.4% to 5.1%. Furthermore, by dipping the substrate in hydrogen peroxide for 48 hours at room temperature, a rough TiO_2 underlayer was obtained, improving charge collection and delivering FDSCs with a PCE of 6.2%.

An alternative way to improve charge collection at the Ti/ TiO_2 interface, consisted in applying the TiCl_4 pre-treatment developed for glass based DSCs.¹⁴² This treatment was applied on a clean Ti foil first and later also on the mesoporous TiO_2 layer, by immersing the substrate in a TiCl_4 solution, followed

by annealing at 450 °C. The flexible DSC made with this photoanode delivered a PCE of 7.2%.

The polishing step can also be realized via a chemical bath, using strong acids such as HF, at times followed by HNO₃.^{110, 143, 144} The surface pre-treatment with HF, together with a photo-platinized CE led to a PCE of 8.1%.¹¹⁰ A hydrothermal treatment in NaOH solution allowed to obtain a PCE of 6.7% on large areas (100 cm²) measured outdoors (incident power of 55 mWcm⁻²)¹⁴³.

By combining several aforementioned pre-treatments, chemical polishing with HF and HNO₃, H₂O₂ chemical bath and TiCl₄ treatment on the oxidized foil, a TiO₂ nanoforest underlayer was obtained onto which complete devices (Ti PE and a plastic CE) were subsequently fabricated as shown in Figure 7. A PCE of 8.5% was obtained, which is considerably higher than the one relative to Ti foil used as received (3.5%) and represents the most efficient flexible DSC on Ti foil under standard illumination conditions.¹⁴⁴

A different way to enhance the performance of titanium based DSCs consists in depositing submicron SiO₂ beads over the TiO₂ (see Fig.3, right). In this way the transparent beads occupy the space previously taken by the opaque electrolyte thereby enhancing the number of photons reaching the active dye-sensitized layer, thus improving the overall transmittance of the electrolyte chamber. With this method a 10% increase in the J_{SC} was observed, resulting in a PCE of 7.1%.¹⁴⁵

Titanium is also interesting in that it allows for simple electrochemical growth of aligned TiO₂ nanotubes.¹⁴⁶

It is interesting to note that we have found only one report of a metal-based solid state FDSC which uses a semi-transparent gold window as top electrode and with a PCE of 0.8%.¹⁴⁷ Finally, the most efficient flexible dye solar cell reported was fabricated on a modified stainless steel foil.⁷³ A thin bilayer of SiO_x and ITO was sputtered on the StS. A hydrothermally synthesized TiO₂ paste was printed by doctor blade and subsequently sintered at 600 °C reaching a maximum PCE of 8.6%.

5. Dyes

Many FDSCs in the literature utilize di-tetrabutylammonium cis-bis(isothiocyanato)bis(2,2'-bipyridyl-4,4'-dicarboxylato)ruthenium(II) (N719) as TiO₂ sensitizer including amongst the most efficient FDSCs currently reported.^{73, 74} Other complexes such as Z907 and the black dye have also been used.^{148, 149} Generally dyes utilized for FDSCs are the same as those developed for glass devices on which there is ample literature^{3, 150}. Recently a heteroleptic ruthenium complex named CYC-B11 was employed to fabricate a highly efficient and stable flexible DSC sub-module thanks to its wide absorption spectrum and hydrophobic side chains.¹⁴⁵ In fact, since the rate of ingress of moisture will be higher for devices with plastic electrodes compared to their glass-based counterparts, it is

generally even more desirable to have stable hydrophobic dyes to minimize the effect of H₂O on the long term stability of these devices.

Dyes with particularly high molar extinction coefficients are also especially desirable for plastic FDSCs since they allow the use of thinner mesoporous TiO₂, which would result in both improved electron collection (due to the TiO₂'s higher transport resistance compared to high-temperature-processed counterparts) and also enhanced resistance to delamination or cracking upon bending.¹⁰¹ Organic dyes and quantum dots (QDs) may also be suitable for this aim.¹⁵¹ CdS/CdSe QDs were used in FDSC delivering a PCE of 3.5%. A double layered TiO₂ PE with a ruthenium dye on top and an organic dye near the bottom delivered a PCE of 6.6%.¹⁰⁵

6. Counterelectrodes

Flexible CEs should be endowed with both good catalytic activity towards the electrolyte redox couple and good adhesion of the catalyst to the substrate³, even when processed at low temperatures (as required for CEs developed on plastic substrates²⁶). In addition, high transmittance of light is mandatory for a CE¹⁵² when using an opaque metal-based photoelectrode (PE)⁷ or for those applications where transparency is sought for aesthetical and/or operational reasons (e.g. BIPV).

So far, a large number of materials have been integrated in devices as catalyst for flexible CEs: platinum-based^{74, 110, 153, 154}, carbon-based¹⁵⁵⁻¹⁵⁸, polymers¹⁵⁹⁻¹⁶², transition metal sulfides^{163, 164}, nitrides^{165, 166}, carbides¹⁶⁷ and oxides¹⁶⁸. Depending on the substrate type (metallic or plastic) and catalyst material, a wide variety of processes have been developed, based on both chemical and physical techniques¹⁶⁹. Most of them are low-temperature and easily up-scalable.

Table 3 summarizes some of the main results concerning flexible CEs and related fabrication processes for both plastic and metallic substrates. An effective CE presents both low charge transfer resistance at the catalyst/electrolyte interface, R_{ct} (i.e. strong catalytic activity) and/or transparency, together with high PCE values when assembled in FDSCs. Further interesting techniques and promising alternative catalyst materials, especially for novel ITO-free solutions, are reported in the following sub-sections. For most of those CEs, high efficiencies are shown when coupled with FTO/glass PEs but should be tested in all-flexible DSCs in the future.

6.1. Plastic counterelectrodes

6.1.1. Platinum counterelectrodes

Similarly to glass¹⁷⁰, platinum is the most commonly utilized catalyst material due to its impressive catalytic properties. So far, sputtered Pt has often been the preferred choice for plastic CEs. In fact, Yamaguchi et al. demonstrated the most

efficient all-plastic DSC using sputtered Pt on ITO/PEN as CE (PCE of 8.1%)⁷⁴. Tuning the deposition time, a highly transparent (almost 70%) Pt layer with a good charge transfer resistance ($10.35 \Omega\cdot\text{cm}^2$) was obtained¹⁷¹, making it suitable for CE-illuminated DSCs with metallic PEs (Fig. 8, top). Konarka/G24 Power Ltd, commercial manufacturer, reported a sputtered Pt CE on ITO/PEN and NREL-certified lab cell efficiency of 7.17%¹³⁹. Although one can prepare sputtered Pt rolls to insert in a R-2-R line, many efforts have gone into finding alternatives to sputtering in order to overcome some of its drawbacks (related to the requirement of high vacuums and costs¹⁷²). Recently, effective transparent and catalytic Pt layers were obtained via atomic layer deposition (ALD) on ITO/PEN, even on large areas¹⁵³. Other simple and low temperature processes such as dipping¹⁷³ and spray coating¹⁰⁷ have given promising results: Pt spray-coated on ITO-PEN as CE coupled with a Ti foil PE yielded a device with state of the art efficiency of 8.5%¹⁴⁴. By simple chemical reduction of Pt precursors, both reflective¹⁷⁴ and very transparent¹⁵⁴ Pt CEs have been obtained. A similar reduction process can be also induced by UV exposure. An R_{ct} as low as $0.66 \Omega\cdot\text{cm}^2$ was obtained by UV processing the Pt precursor on a TiO_2 template. This CE (76% transparency) assembled in a Ti/plastic FDSC delivered a PCE of 8.12% which is amongst the highest values reported.¹¹⁰ Utilizing a simple screen printed Pt precursor paste on ITO/PEN and powerful UV irradiation, Zardetto et al.

demonstrated the first all UV processed DSC and also the suitability of such method for large area devices without the need for additional TiO₂ templates (Fig. 8, bottom)¹¹⁶.

Electrochemical deposition (ED) of platinum has received also considerable attention since Kim et al. proved its suitability for plastic substrates¹⁷⁵ and Ito et al. reported a PCE 7.2% for a back-illuminated metal-plastic DSC equipped with such a CE¹⁴². Changing deposition parameters¹⁷⁶, and even blending different catalysts precursor materials¹⁵², allows one to tune the optical and catalytic characteristics of the layer with the ED technique delivering low R_{ct} and superior transparency (beyond 75% on ITO-PEN (Fig. 8, middle)) with less material consumption¹⁵². Electrodeposition is a simple, fast and inexpensive process, easily up-scalable for metallic substrates (SoloPower Systems Inc. has implemented it in its CIGS production line¹⁷⁷). Additional efforts are required to prove and validate the long term stability of this kind of CE, mainly related to adhesion to the TCO and/or possible poisoning¹⁷⁸, and to include the process in a roll-to-roll production line, solving the problem of non-homogeneous deposition caused by voltage drop especially on the more resistive ITO/plastic substrates. Reference¹⁷⁹ reports a method to overcome this issue by depositing a conductive grid necessary to maintain uniformity of the voltage of the substrate during the ED process. A large area parallel module (22 cm²) in which the CE was obtained

by ED of Pt in a few seconds on a plastic/ITO substrate, covered by conducting grids which subsequently functioned as current collectors in the finished device, delivered a PCE of 2.7% at 1 Sun and 3.0% at 0.2 Sun¹⁷⁹.

6.1.2. Alternative counterelectrode materials

Apart from Pt, a variety of other catalytic materials have been electrodeposited on conductive plastic substrates^{159, 161, 163, 164, 180}, including cobalt sulfide (CoS)¹⁶³, PEDOT¹⁶⁴ and carbon¹⁸¹. CoS resulted in a semi-transparent CE with an R_{ct} of 1.8 $\Omega\cdot\text{cm}^2$ and a front-illuminated device PCE of 6.5%, withstanding also a 1000 h ageing test at 60 °C under 1 Sun illumination¹⁶³. PEDOT, coupled with a disulfide/thiolate (T^2/T^-) based electrolyte, showed a higher R_{ct} (15.2 $\Omega\cdot\text{cm}^2$) but still a remarkable PCE of 5.9% and good shelf life after 1000 h storage¹⁶⁴. Semitransparent PEDOT has been also deposited by electropolymerization on ITO/PEN yielding a PCE of 8% when integrated in a front-illuminated device based on I^-/I^{3-} electrolyte and N719 dye¹⁵⁹. Ellis et al. succeeded in electrodepositing PEDOT from an aqueous micellar solution, even on a 9 x 9 cm^2 ITO/PEN substrates¹⁸². Pt nanoparticles can also be used to enhance the performance of otherwise less catalytic but cheaper materials¹⁸⁰, resulting in lower Pt loading and overall cost reduction and have been sprayed on single walled carbon nanotubes (SWCNTs)¹⁸³ and spin coated on polyaniline (PANI)¹⁸⁴ on

ITO/plastic substrates. By printing a composite paste prepared by adding TiO₂ nanoparticles to an aqueous dispersion of PEDOT-PSS and a slurry of ITO over an ITO/PEN substrate, a semi-transparent Pt-free CE was obtained and used in DSCs that delivered a PCE only slightly lower than devices with sputtered Pt CEs¹⁸⁵. Such low T (110-130 °C) printable solutions, including a carbon based gel with excellent flexibility can represent a very low cost option for R2R fabrication of large area CEs in plastic/plastic devices¹⁸¹.

Due to the issues of brittleness and stability of ITO (due to interaction with the components of the electrolyte), TCO-free counterelectrodes are being investigated including abundant carbon based materials (see Fig.9). The challenge is to guarantee sufficient conductivity and high surface areas which often means combining different materials together. PEDOT becomes more conductive by tuning the PSS concentration and can be easily printed or applied by electro- and solid state polymerization^{160, 186}. Its conductivity and catalytic action can be respectively enhanced by silver nanowires embedded in the substrate and by TiO₂ nanoparticles¹⁸⁷ or by honeycomb-like silver grids printed on the plastic substrate¹⁸⁸. A cheap graphite substrate covered by a large-effective-surface-area polyaromatic hydrocarbon layer and coupled with a FTO glass-based PE in a device delivered a PCE of 8.63%¹⁸⁹. The more evident drawback of relatively thick carbon based layers like graphite is their very low or null

transparency^{168,190,191} which makes them unsuitable for back-illuminated devices such as those fabricated on opaque metallic PEs. Graphene seems promising and can be deposited on substrates like polyimide (PI) via different routes based on chemical reduction^{190,192}: the resulting CEs exhibit highly catalytic performance, thanks to the porous structure with numerous edges of the graphene film (Fig. 9, bottom-left), equaling the PCE of sputtered DSC with Pt CEs. Exfoliated graphite served as substrate for an electropolymerized PEDOT:PSS layer ($0.78 \Omega\cdot\text{cm}^2$) used in a solid-state DSC yielding a PCE of 5.7%¹⁹¹ (Fig. 9, top-right). Spin coated PEDOT on conductive graphene/PET substrate showed more than 70% transmittance and passed bending tests (Fig. 9, top-left), confirming its flexibility and strong adhesion to the substrate¹⁹³. SWCNTs deposited on PET by a simple press-transfer method¹⁵⁵ exhibit impressive R_{ct} ($0.72 \Omega\cdot\text{cm}^2$) for a $\text{Co}^{2+/3+}$ electrolyte. SWCNTs have also been printed on PVC using a low temperature ink delivering a low R_{ct} ($2.7 \Omega\cdot\text{cm}^2$) when coupled with a thin spin-coated PEDOT-TsO layer and a similar PCE compared to thermally platinized CE¹⁵⁶. Conductive carbon on PI can act as a conductive underlayer for sprayed vanadium nitride (VN), tungsten oxide (WO_2) and titanium carbide (TiC)¹⁶⁸, which can also be printed¹⁶⁷. More recently, a simple low temperature method was demonstrated to obtain a free-standing paper-like polypyrrole (PPy) membrane, based on self-assembling from PPy nanotubes dispersed in a suspension under a vacuum

atmosphere¹⁹⁴. Such a flexible ITO- and Pt-free CE exhibits good catalytic performance ($5 \text{ } \Omega \cdot \text{cm}^2$) thanks to its porous structure and high specific surface area, leading to a PCE of 5.27% when integrated in a cell.

6.2. Metallic counterelectrodes

Constraints on maintaining low temperatures, high-transparency and the concerns on the stability of ITO can be lifted by adopting metallic foils (or meshes/fibers) as CE (although they are then necessarily transferred to the plastic PE). As already mentioned, metals possess lower sheet resistance compared to ITO but are more prone to corrosion in the aggressive I^-/I^{3-} electrolyte medium^{45,46,4} with titanium showing the highest stability.

Pt is the preferred catalyst used even for metal CEs. Deposition techniques range from sputtering^{74, 195}, even on fiber-shaped substrates¹⁹⁶, to electroless¹⁹⁷ or electrochemical deposition¹⁹⁸, and physical vapour deposition⁵¹. Sputtered Pt on Ti foil gave a certified record of 7.6% PCE when integrated in a FDSC, as reported by Yamaguchi et al. in their work on the TiO_2 PE compression method⁷⁴. Electroless deposition of Pt on nickel and StSt substrates gave a R_{ct} of $\sim 2 \text{ } \Omega \cdot \text{cm}^2$ and almost 7% PCE in DSCs assembled with PEs on FTO glass¹⁹⁷. Xiao et al. demonstrated simple and fast electrodeposition of Pt over a Ti mesh in an all-metallic large-area (80 cm^2) DSC, with a PCE of 6% under 55 mW/cm^2 outdoor

natural light irradiation¹⁹⁸. By the same method, they also deposited PEDOT on a similar mesh, obtaining 6.33% PCE over 100 cm², proving the suitability of conductive polymers as catalysts on large areas¹⁹⁹. In the same vein, an 11 μ m-thick polyaniline (PANI) film was electrodeposited on StSt foils, which gave an R_{ct} of 6.8 $\Omega\cdot\text{cm}^2$ and a device PCE of 7% (PE on FTO glass)¹⁶². Transition metal nitrides (and carbides) were investigated for use as CEs. Highly ordered titanium nitride (TiN) nanotube arrays, prepared by anodization of a Ti foil and subsequent nitridation in an ammonia atmosphere demonstrated high catalytic activity, leading to a PCE of 7.73% (with an FTO/glass PE)¹⁶⁶; sputtered molybdenum nitride (Mo₂N) and tungsten nitride (W₂N) on Ti foils also showed a very low R_{ct} , achieving almost 6% PCE with a FTO/glass PE¹⁶⁵. TiC, WO₂ and VN were deposited on Ti substrates by simple spray coating of their respective precursors, reaching lower R_{ct} and higher PCE than in the case of the same catalysts on plastic substrates (conductive carbon on polyimide)¹⁶⁸. Low-cost carbon-based materials also attracted much attention: carbon nanotubes and carbon nanofibers were spin coated on a Ti foil and post treated with an ethanol flame synthesis method, showing high catalytic activity thanks to a peculiar hierarchical porous structure (Fig. 9, bottom-right) and leading to a PCE of 6.5%²⁰⁰; vertically oriented graphene was obtained via plasma enhanced chemical vapour deposition (PECVD) on StSt substrate with encouraging results ($R_{ct} = 7.3 \Omega\cdot\text{cm}^2$, >5%

PCE)¹⁵⁷; a carbon aerogel deposited on StSt mesh gave $4.8 \text{ } \Omega \cdot \text{cm}^2 R_{\text{ct}}$ after compression and a PCE of 9% in a glass-based DSC²⁰¹. Combining non carbonaceous catalysts, e.g. Pt nanoparticles or CoS, with carbon based materials such as MWCNT is another explored route^{202,203}.

7. Electrolytes

Currently the I^-/I_3^- redox mediator²⁰⁴ is the most common electrolyte for FDSCs in either acetonitrile (ACN) or metoxypropionitrile (MPN) solvents.² The latter has a higher boiling point and viscosity, fundamental to avoid electrolyte leakage/evaporation and to assemble long-lasting devices. The former has a low viscosity which enhances the mobility of the ions and thus photocurrents. Optimal iodine concentration, appropriate additives and solvents are crucial to obtain highly efficient or highly stable DSCs. Different compositions are often used depending whether tests are aimed at obtaining the highest efficiency or rather long term stability (see Table 4). The amount of I_2 (which determines $[\text{I}_3^-]$) defines the final concentration of the redox couple, since the iodine salt is generally about an order of magnitude more concentrated. Although it enhances the conductivity of the electrolyte, too much iodine raises recombination losses and the unwanted absorption of the incoming light (an important issue especially for back-illuminated DSCs). The appropriate concentration depends on solvent viscosity,

TiO₂ porosity, chamber thickness and also on the catalytic properties of the CE.^{205, 206}

Two classes of iodine salts are typically used, alkaline inorganic salts or organic salts based on imidazolium or tetrabutylammonium. ITO/plastic substrates are more unstable compared to FTO/glass regarding both the resistance to corrosion against acidic solutions and the Li⁺ inorganic cation.^{67, 125} Inorganic cations enhance charge injection in TiO₂ by increasing the driving force and thus enhance J_{SC},²⁰⁷ but can degrade the ITO. Tetrabutylammonium iodide (TBAI) can substitute Li⁺ since it has been shown to enhance both the PCE and the device's durability compared to a propyl-methyl-imidazolium iodide (PMMI) or the LiI-based electrolyte, thanks to its passivation of the TiO₂ surface.^{67, 208} Others Li⁺-free additives used to improve cell performance by modifying the TiO₂ surface are 4-tert-butylpyridine (4TBP), N-Methylbenzimidazole (NMB) and guanidine thiocyanate (GuSCN). From the contrasting literature available it is not yet clear if the effect of 4TBP is as effective or even detrimental in FDSCs compared to when used in glass DSCs^{145, 149, 209}. NMB can easily substitute 4TBP in flexible cells, since it has a similar effect and no observed incompatibility with ITO.²¹⁰ GuSCN is added to the electrolyte formulation to increase charge injection and J_{SC} and to passivize TiO₂ recombination sites enhancing both performance and stability,²¹¹ an effect enhanced in combination with NMB.²¹⁰

Liquid electrolytes have been used to test the stability of FDSC under light soaking or temperature and humidity stresses.^{67, 145, 208} However no quantitative extraction of acceleration factors for estimating operational lifetime was carried out (in analogy to glass based devices^{212, 213}). For plastic DSCs a TBAI-based formulation with NMB in MPN allowed to maintain 75% of the maximum PCE after 1000 hours under a light soaking test at 1 Sun and 60 °C.⁶⁷ A titanium foil FDSC with PMII based electrolyte with 4TBP in MPN, maintained a more stable performance, with a 20% PCE loss after 1500 hours of light soaking test (1 sun, 50 °C).¹⁴⁵

In order to improve cell performance and stability a gelling agent^{148, 191, 214}, either inorganic or polymeric, can be added to electrolyte formulation and then deposited. At times polymer matrices can be either grown on the PE and then filled with electrolyte or dipped in electrolyte and then transferred onto the PE. Gelification can be considered a route not only to avoid electrolyte egress for enhancing lifetimes, but also towards processing with large area techniques such as screen printing²¹⁵⁻²¹⁷.

Silica nanoparticles are a well-known gelling agent for rigid DSCs.²¹⁸ A light-scattering gel-electrolyte with commercial SiO₂ nanoparticles and submicron mesoporous silica nanoparticles (MSNs) was employed to improve J_{sc}.²¹⁹ The mesoporous morphology of the MSNs helped the diffusion of the ionic species

while maintaining the light-scattering properties. Addition of P25 TiO₂ nanoparticles to the liquid based electrolyte improved ion mobility and the PCE more than the SiO₂ nanoparticles did.⁷⁸ The effect was even more evident in a solvent-free binary ionic liquid formulation, where the PCE was improved from 1.6% to 2.8% by adding 17.5% of P25. The latter formulation showed good stability, maintaining >97% of the initial efficiency after 500 hours of light soaking as shown in Figure 10. Due to the higher permeation rates of vapours in and out of FDSCs, developing very low-volatility/high-boiling point electrolytes may be even more important compared to glass-based counterparts. Electrolytes, with boiling points even above 280 °C, have proven to enhance stability of glass DSCs²²⁰ and should be tested on flexible DSCs too. Tailored formulation of the electrolyte can be considered when trying to combat corrosion of metal substrates other than Ti. In fact additives/compounds contained in the electrolyte (e.g. 4-tertbutylpyridine⁵¹, nitrogen containing heterocyclics²²¹) can help in inhibiting corrosion to certain metals like StSt .

Besides the iodine redox couple, Cobalt complexes have been employed in electrolytes for glass-based DSCs delivering increased Voc and even efficiency²²²⁻²²⁴. Cobalt-based electrolytes have been proven to be compatible with plastic counterelectrodes^{155, 182, 186} but systematic studies on performance and stability in full FDSCs should be carried out to exploit the potential of these formulations.

These electrolytes have high transmittance in the visible range which can enhance the photon flux arriving on the PEs in metal based cells.

8. Flexible large-area dye solar cell modules

The up-scaling from small laboratory test cells (as those described in the previous sections) to those large-areas required in applications (to deliver the necessary electrical power) is not trivial. It requires development of effective module architectures and ultimately of high-throughput, high-yield, low-cost manufacturing lines.

8.1. Module architectures

Since the sheet resistance of the transparent conductors acting as electrodes are relatively high, developing a module²²⁵⁻²²⁹ entails integrating a number of cells on a common substrate and interconnecting these together⁶. To minimize resistive losses due to the TCO, cells are usually shaped as rectangular stripes whose optimal width depends on the sheet resistance of the ITO, the efficiency of the cells, and illumination conditions but are generally in the few-mm to ~1 cm range^{20, 230}. Current collecting fingers or vertical connections are usually added to the long side so as to also diminish resistive losses. Connections can be in series for increasing the module voltage (keeping the currents low) or in parallel (current output scales with the module area). Module fabrication requires developing

vertical connections (Z-type series architectures), current collection grids (parallel architectures) and their protection, evaluating the effects of sheet resistance of the substrates on performance, designing the most efficient layout depending on illumination conditions, and other issues such as electrolyte filling and cell sealing. The different architectures developed, primarily on glass include parallel modules,²³¹ W-type series interconnections,^{20, 227} Z-type series interconnections,^{20, 230} and monolithic modules.²³²⁻²³⁴

Compared to glass-based devices, the literature on modules on flexible substrates is limited. Arakawa *et al* developed a fully plastic parallel sub-module (10 cm x 10 cm) with Ti current-collecting grids, static compression of the TiO₂ photoelectrode and a sputtered Pt CE.²³¹ Instead, parallel modules developed with photoelectrodes on metallic foils (see figure 11) use arrays of rectangular cells with a silver collecting grid printed on the plastic counterelectrode. A few papers are reported in the literature, developed on Ti or StSt, with efficiencies between 3-7%,^{153, 179, 235-237} where performance depends also strongly on the foil surface pretreatment applied.

Regarding the Z-type series architecture, a large 30 cm x 30 cm fully-plastic module integrating 10 unit cells via vertical interconnections between cells was exhibited in Expo Aichi 2005 by Ikegami *et al*. 3.5 cm x 30 cm rectangular cells were interconnected along their long edge with a double-sticky conductive tape

applied on printed conductive silver busbars treated at temperatures < 120 °C. The TiO_2 mesoscopic titania layer was fabricated following the low temperature procedure introduced by Miyasaka *et al.*,²³⁸ while a titanium/platinum alloy was sputtered on PEN/ITO CE.²⁷ Metal based DSC series modules do not follow the integrated approach of the Z-type series of depositing all the active and conductive layers simultaneously on common substrates. This is because a common metal foil would short all the cells together. Fabrication of stripe cells and their subsequent electrical connection and integration (lamination) together on (with) flexible insulating substrates yield series architectures such as those already commercially manufactured by G24 Power Ltd. Their large area modules (> 200 cm²) at the time of writing consisted in Ti-based PEs and plastic film CEs¹³⁸ with an unpublished PCE of 4.97% at 1 sun ¹³⁹ and, as will be detailed in section 10.1 (operation in relevant environments), with high power densities in indoor lighting, outperforming other main competing flexible photovoltaic technologies.

The first example of W series-interconnected module, which requires no additional metallic interconnects (such a Z architectures) or collecting grids (such a parallel modules), but requires shaping neighboring cells in two different sizes in order to match the currents flowing through all cells (due to the fact that, for each pair, one cell is illuminated from the PE and its up-side-down neighbor from the CE) was recently demonstrated. Both electrodes were treated by UV-

processing which permitted platinization and post-treatment of the TiO₂ on a common plastic substrate simultaneously yielding a PCE of 2.3% at 1 Sun and 2.7% at 0.3 Sun on an active area of 16.4 cm².¹¹⁶ A selection of results of FDSCs modules are summarized in table 5.

Compared to conventional architectures, the development of highly conductive metal meshes has led to a novel approach based on the development of very large area single cells in order to overcome the limit of the considerable size of the inactive areas remaining between cells (after fabricating modules as a multitude of narrow rectangular cells). Single flexible devices with an active area of over 100 cm² were demonstrated. TiO₂ nanoparticles, or 3-D interpenetrating network of TiO₂ nanowires were prepared on Ti as PEs. PEDOT-Pt or Pt-single wall carbon nanotubes (SWCNTs) were deposited on Ti mesh for highly transparent and high catalytic CEs. These backside-illuminated large-area (100 cm²) devices delivered high efficiencies for such areas in outdoor conditions (at 0.55 sun) of 6.69% and 6.43% respectively.^{143, 239}

8.2. Large area manufacturing

The industrialization of FDSC technology passes also through the tackling of some important technological challenges related to large-area manufacturing, high throughputs and low-cost materials and processes. Industrialization of FDSCs, such as those sought or implemented by companies or centers operating in the

field, often aim to, or have already, set up a continuous line for the manufacturing of flexible modules. Similarly to the flexible OPV field, roll-to-roll (R2R) fabrication can sustain high volume production of large area devices²⁴⁰ whilst reducing costs per m². This review has attempted to cover not only the materials but also the coating, printing and post-processing options for the two functionalized electrodes (i.e. PE and CE) in previous paragraphs, so will not be repeated in this section. Apart from these, other issues pertaining industrial production of modules should be tackled. For example, we have seen that, for the Z and parallel architectures prototypes developed in the academic literature, low-temperature printable silver pastes are often utilized. Their mechanical stability and resistance to delamination after numerous bending cycles is still to be demonstrated. A further important issue in large volume manufacturing is to streamline the process of module assembly. It is thus interesting to delve into the patent landscape to have an idea of some of the solutions adopted for the production of FDSC modules. A number of these pertain to assembling strategies with a metal foil photoelectrode.

For instance in reference²⁴¹ a method is disclosed for the mass production of identical, rectangular-shaped FDSCs. A plurality of electrodes are pre-formed from a common substrate and are cut and separated at a later stage (e.g. by water jet or laser cutting). After the cells are finished they can be incorporated into a semi-

rigid printed circuit board and interconnected according to a Z-series architecture²⁴².

References^{243, 244} disclose R-2-R methods to form a Z series-connected module from a plurality of single stripe cells. All the photo-electrodes are processed (TiO₂ deposition in rectangular stripes, sintering and dye application) over the same metallic substrate²⁴⁵. The substrate is successively divided into separated metallic strips (each corresponding to the PE of the unit cells), and then interconnected and sealed on top with a single, Pt-coated, conductive and transparent plastic substrate, i.e. the CE which had its ITO scribed away between the strips in order to electrically insulate the CEs of each cell. Figure 12 (top) shows part of the fabrication process. The same patent²⁴⁵ also proposes various methods to obtain reliable Z-series interconnections between the cells including the use of soldering irons to connect PE and CE, whilst in reference²⁴⁶ interconnections are implemented by wires coated with a surrounding layer of a metal that possesses a low melting temperature so that, upon lamination at appropriate temperatures, the metal flows helping to forge a more durable and effective contact between the metal PE and the plastic CE (see figure 12, middle). Reference²⁴⁷ discloses a method to realize fully plastic FDSCs and joining them utilizing a fixing member, which is generally conductive and clamps, in some sections, both plastic substrates (see figure 12, bottom).

It is interesting to note that due to the nature of metallic substrates (for which electrical isolation by cutting is the easiest option) and the difficulty in maintaining a sturdy vertical connection by simple printing like in glass based modules (due to the laxness of thin plastic films) the examples described above typically fabricate a plurality of cells first and then interconnect them together subsequently, differently from the typical integrated manufacturing on common substrates options adopted in glass based devices.

9. Encapsulation and lifetime

With a view to its operation as a product, the modules' architecture, geometry, interconnections and active materials are not only designed to maximize power output but have to be able to sustain performance over the lifetime of the application²⁴⁸⁻²⁵². We have seen in the previous sections that for the latter, electrolytes and dyes play a crucial role. Devices also require protection from extrinsic causes of degradation, i.e. moisture and oxygen ingress from the outside which can cause dye desorption, electrolyte degradation (e.g. bleaching), and also leakage/evaporation from the inside. Thus lifetime requires a two-pronged approach: stable active materials combinations and effective encapsulation. The latter (see figure 11, right) typically starts with a reliable primary sealant, which is applied at the perimeter of the active areas, bonding together the two electrodes of

the sandwich structure, defining the thickness and volume of the electrolyte chamber, often protecting the metallic interconnects (collecting grids in parallel modules and vertical interconnections in Z series architectures) from coming into contact with the corrosive electrolyte whilst also preventing its egress. Additionally a secondary sealant and/or barrier layers/laminates are applied to prevent or diminish permeation of oxygen and water vapour. Primary sealants for DSCs are typically thermoplastic polymer films^{61, 248, 253-255} or even printable resins/glues^{228, 256, 257}. For FDSCs, the most commonly utilized are of the former commercial thermoplastic type, e.g. Bynel and Surlyn. Since Surlyn cannot withstand sustained temperatures much higher than 60 °C, which is too low for outdoor conditions²⁵⁰, Bynel is more appropriate for such applications^{258, 259} while Surlyn can remain a good choice for indoor use, where temperature and humidity conditions are more moderate. In fact, plastic modules using Surlyn demonstrated 220 hours stability, in dark under accelerated ageing tests (55 °C and 95% humidity)²⁶⁰, while a cell with the same LiI-free electrolyte, the same sealing and a glass-based CE showed a lifetime of 800 h under light irradiation (1000Wm⁻²) at 50 °C. Very promising results are reported by Lee et al.²³⁶ where a Ti/plastic sub-module with a low volatile electrolyte and a wide absorption spectrum CYC-B11 dye was tested under 1 Sun at T=50 °C. After 1560 h the sub-module PCE maintained 80% of its initial value (see figure 13)

In a glass-based DSC, it is the glass substrates that act as exceptionally good barriers: exchange with the outside environment is limited to the very thin perimeter boundary (and electrolyte filling hole) of the permeable primary sealant between the two glass plates. But when the relatively permeable plastic sheets replace glass, the areas and pathways enabling permeation of gases increases tremendously. Using a metallic sheet as substrate for one of the two electrodes can halve the problem without solving it. A plastic substrate having an adequate water vapour transport rate (WVTR) is required¹⁰ to ensure a stable and durable encapsulation, crucial for FDSCs to move quickly ‘from the laboratory bench to the factory gate’, in the same vein as for flexible organic photovoltaics and electronics (e.g. OPV, OLEDs, TFTs). Moreover plastics, especially PEN, suffer from long-term UV irradiation, which alters their optical transmittance (yellowing)²⁶¹ and also leads to dye and strong electrolyte degradation (bleaching)^{252, 262}. Therefore, UV barriers become necessary⁷.

So far, in the field of FDSCs, apart from a small number of publications²⁶³, most works on stability and long term durability have focused on alternative cell materials (e.g. less volatile solvents and/or quasi solid electrolytes, avoiding the use of LiI or other inorganic cations to prevent ITO degradation, developing more water resistant devices^{7, 264, 265} (see also sections on dyes and electrolytes) more than on encapsulants and/or barriers.

On the contrary, encapsulation for OPV has become a hot topic, mainly because the monolithic structure of its modules entails that the top of the device is exposed directly to air if not immediately sealed (whereas for FDSCs most architectures have an ITO-coated plastic and/or a metallic substrate enclosing the active layers on both sides which already acts as an initial barrier). Krebs et al.^{266, 267} utilized commercially available low-cost materials with good barrier properties ($WVTR=0.04 \text{ g m}^{-2} \text{ day}^{-1}$, oxygen transmission rate $OTR<0.01 \text{ cm}^3 \text{ m}^{-2} \text{ bar}^{-1} \text{ day}^{-1}$) for their OPV modules and often incorporated a UV-filter film²⁶⁸, suitable for roll-to-roll lamination evaluated in a 900 h lifetime test at $35 \text{ }^\circ\text{C}$ ²⁶⁷.

As mentioned before, in theory, even for flexible DSCs the best barrier could consist in glass. Some important glass suppliers such as Corning and Schott have developed ultra-thin (25 - 100 μm) flexible glass for electronic applications (touch screens and similar) even suitable for R2R fabrication. However, these have not yet been tested in FDSCs in the literature. In practice glass is a brittle material so that the development of rugged permeation barriers which are at the same time transparent and flexible without adding significant cost to the final product is ongoing and a complex undertaking. An effective strategy to implement for FDSCs may consist in drawing on the experience of the flexible OPV and OLED fields. Huang et al.²⁶³ demonstrated sputtered aluminum oxynitride (AlO_xN_y) on PEN to be a good barrier film ($WVTR=0.02 \text{ g m}^{-2} \text{ day}^{-1}$): flexible DSCs equipped

with such a layer sustained 50% of its initial PCE even after 300 h of storage. In February 2014 G24 Power Ltd. ensured 3 years lifetime in an attuned environment for its modules protected by a vapour barrier polymer front sheet with high light transmission¹³⁸. Further and in-depth studies have to be addressed to evaluate the long-term stability of encapsulated devices, mainly during operation. Since the required WVTR to assure sufficient protection for thousands hours of operation should be in the 10^{-3} - 10^{-6} g m⁻² day⁻¹ range^{269, 270} techniques such as ALD and sputtering are continuing to be developed as effective processes for depositing barrier layers, even compatible with a roll-to-roll manufacturing. A multi-layer barrier approach can be an effective solution^{42, 271}. Fahlteich et al. reported two layers of metal oxide, e.g. aluminum oxide or zinc-tin oxide²⁷², separated by a hybrid polymeric layer⁴², and deposited by sputtering and magnetron-PECVD. Such multilayer stacks show very good permeation barrier properties, high optical transmission, and good UV, mechanical and temperature stability which are also required for FDSCs⁷ and should therefore, with these, be tested.

10. Operation, applications, costs and markets

10.1. Operation of the technology in relevant environments

As mentioned in the preceding sections, under outdoor or solar simulator illumination conditions, considering only module size (which customarily present lower performance per unit area compared to the small laboratory cells (see Tables 1-3 for these) as for all PV technologies), the highest PCEs reported (see Table 5) over these large (active) areas are 7% with PEs on Ti foil^{236, 273} and 4.5% on plastic²⁷⁴. Promising stability has been reported under certain light soaking conditions, as those shown in figure 12, but which nevertheless needs to improve especially under real changing (high illumination, temperature excursions, UV and humidity) outdoor conditions. Under the latter, a recent study²⁷⁵ implemented the peculiar property of FDSCs of being able to be conformed to curved surfaces and analyzed the energy produced by a large area 8 cm² cell over the course of a diurnal cycle: compared to flat devices, curved cells delivered up to almost 10% enhancement of energy produced per unit of occupied projected area demonstrating the attractiveness and possibilities of portable, light-weight and conformal FDSC technology.

Recently, a number of studies²⁷⁶⁻²⁸⁰ have pointed out that DSCs represent the best-performing technology for harvesting energy from indoor illumination. FDSCs deliver more power per unit area than even flexible OPV and amorphous silicon under 10²-10³ lux illuminance^{138, 276} (a-Si previously being considered the most suitable for indoor light harvesting). The remarkable indoor performance of

DSCs is due to a combination of factors: better match of the illumination spectra with the external quantum efficiencies of DSCs (compared to the sun, for example, fluorescent lamps emit a much higher fraction of their light in the visible range which is where most dyes absorb strongly), very good (and in selected ranges superior) performance under low levels of incident power and oblique angles of incidence^{229, 281}. G24 Power Ltd. (or G24i at the time), at the Dye Solar Cell Industrialization Conference 2010 (DSC-IC 2010), presented a doubling in power density output by changing part of the materials and chemistry in the DSC system, from 3.43 to 6.73 $\mu\text{W}/\text{cm}^2$ at 200 lux. In early 2014, these power density values advertised on their website for their product devices were also accompanied by a lifetime of 3 years in the attuned indoor range (50-2000 lux and operating temperatures of 10-50 °C). At the EuroNanoForum conference in 2013 their indoor modules (200-1000 lux) outperformed a-Si ones (showing very high efficiencies estimated to be around 15% notwithstanding the difficulty of carrying out indoor measurements and lack of existing standard protocols for these). Always indoors, Miyasaka et al. demonstrated high 110V voltage output delivered by a very large 1 m \times 2 m flexible DSC panel composed of ninety six 10 cm \times 10 cm plastic/plastic sub-modules¹⁰¹.

10.2. Applications, costs and markets

Due to both the remarkably high power densities generated, and the stability issues which still need to be solved to guarantee long-lasting devices in all outdoor conditions, the immediate ‘natural’ target market for FDSCs is represented by indoor low-power applications. G24 Power Ltd., relatively recently has seemed to embrace this business opportunity, even changing its web site, highlighting its offer for indoor applications. The technology is suitable for recharging consumer electronic devices (for many of these, current lifetimes are similar to those of FDSCs), powering wireless devices (sensors, actuators, displays) for improving the management of indoor environments (energy, comfort, information, etc.), making these (and fitted products) “smart” (e.g. in domotics/home automation) and for electronic devices utilised for retail trade (ePrices, RFid Tags, POS shelf Talkers, Powered Smart Card)¹³⁸. Depending on location, placement and living conditions, the technology is also envisaged to compare favourably with wired energy in terms of installation costs and flexibility; with disposable batteries for maintenance costs, functionality and environmental impact, with some other mechanical (vibration), and thermal energy-harvesting sources in performance/cm³, and with other flexible photovoltaics (see section above) such as a-Si delivering greater power in low level light conditions²⁷⁶. It can also be tailored in form, dimensions and colour for custom projects²⁸² and being thin, lightweight and conformal is more easily

integrated into the electrical device it needs to power (opening routes to easy-to-install self-powered electronics and to fit-and-forget sensors with negligible maintenance costs). In 2013 Dyesol Ltd. and Printed Power teamed up to integrate DSCs (not specified, in the press release, whether with rigid or flexible substrates, both of which Dyesol has had interests in) with printed batteries and power management systems to create fully integrated combined energy generation and storage devices²⁸³.

In early 2014 a number of commercial products powered by FDSCs onto which they were integrated were available on the market. Amongst these we mention for instance the e-reader cover by Leia Media¹³⁸ the bluetooth keyboard by Logitech²⁸⁴, the indoor cylindrical gas sensor, by Argus Security²⁸⁵ and motorized shades by Skyco²⁸⁶.

Market studies support these intuitions and foresee strong expanding business opportunities in these fields (see Figure 14) and in the emerging market of the Internet of Things, where billions of physical devices will be interconnected together (in a network). According to projections by IDTechEx, the market for DSCs (in general) will slowly grow to over \$130 million in the next decade²⁸⁷ starting out with indoor low-power portable products to much larger outdoor applications. Markets will expand in tandem with continuous improvement in performance and lifetime. In fact the roadmap for FDSC development aims to

satisfy the harsh demands of continuous outdoor use, and, thus, to being applied for example on clothes, shelters and ultimately BIPV which represents a huge market²⁸⁸.

The success of future penetration of FDSCs into such promising markets also depends on reducing costs, which vary depending on application but a target ≤ 1 $\$/W_p$ being common to many PV technologies^{254, 289}). As we have seen in the previous sections, the choice of abundant, low-energy materials/processes and the implementation of continuous high-throughput roll-to-roll production are promising strategies to follow for reducing product costs⁶. Cost analyses for FDSCs mainly refer to cost evaluations for OPV²⁶⁶ or glass-based DSCs since they share many common components^{254, 289}. Compared to glass DSCs significant reduction of costs in substrate components was estimated both for plastics and metal foils (especially the more abundant ones like aluminum)^{6, 7} although one needs to consider the cost of additional permeation barriers which will also depend on the sensitivity of the active materials to gas ingress. Considering production capacities of 10 MW/y, one can estimate costs well below 100 $\$/m^2$ including manufacturing, materials, labour, capital and overheads^{289, 6, 290}. Notwithstanding the difficulty of making reliable future cost estimates for a new technology, an outdoor efficiency of 5% brings these in the 1.5-2 $\$/W_p$ range and below 1 $\$/W_p$ for efficiencies in the 8%-10% range. Clearly, the roadmap for

large-scale penetration of FDSCs must not only maximize the market potential of its peculiar characteristics (conformal, light-weight, flexible, customizable in forms and colours etc.) but simultaneously achieve ever higher targets pertaining its efficiency (in relevant environments) and costs, together with the appropriate lifetimes required by each application.

11. Alternative device architectures and concepts

Most of the device architectures developed in FDSCs, and encountered in the previous sections, have been of the sandwich type, based on plastic substrates coated with TCOs and/or metallic foils which either need to be scribed or cut in the process of manufacturing series-connected modules. When reviewing the sections on substrates and electrodes, we have already come across the growing literature on TCO-free and metal mesh-based FDSCs for the fabrication of both PEs and CEs^{7, 32, 54-57, 291}. Figure 15 (top left) shows the microcopy of a StSt mesh onto which the mesoporous TiO₂ layer was deposited after a 3-cycle dip and subsequent spray coating of a TiO₂ solution followed by sintering at 500 °C for 15 mins⁵⁴. The CE consisted of a 0.05 mm thick Pt foil. 6.1 % efficient devices were obtained by stacking together a TCO-free PET insulating film, a sheet of flexible mesoporous titania supported by a metal mesh, a gel electrolyte sheet and a Pt/Ti sheet.⁵³

The use of metallic meshes opened up the possibility of fabricating TCO-less devices in a three-dimensional cylinder architecture (Figure 15, top right)⁵⁵. The flexible solar cell consisted in a porous silicone tube (A), a titanium-coated stainless metal mesh tube working as a CE (B), a gel electrolyte tube based on a PTFE sheet (C), a dye sensitized mesoporous titania tube (D) fabricated on a protected stainless metal mesh tube working as PE (E), and a transparent plastic tube (F). With this configuration, the total electric energy output (generated in a day) reported was 1.3 times larger than that of the TCO-less flat device.

Another different architecture compared to the common planar independent PE/CE sandwich structure of figure 2 was proposed by Fu et al. (Fig. 15, bottom right)²⁹². In this structure, a platinized flexible Ti foil was used as the bottom substrate and acted as the CE onto which a porous ZrO₂ spacer layer was coated. Subsequently a thin Ti film was deposited (acting as the PE) and also a mesoporous TiO₂ layer with electrolyte injected into the porous matrix finally completing the device (capped by a top transparent substrate to contain the liquid but with no electrical functions). This TCO-free architecture delivered a PCE of 4.2%. Cha et al.²⁹³ developed another TCO-free design, in which the PE, a conductive metal mesh, and the CE, were bonded to a glass fiber paper, which was filled with electrolyte maintaining its PCE even when bended to a 2cm radius of curvature.

Flexibility and miniaturization were taken to remarkable levels with the development of wire shaped FDSCs (see figure 15, bottom left). ITO-free, wire-shaped FDSCs were formed by twisting two fiber-like electrodes (one acting as PE and the other as CE) in a helic-like structure^{32, 294}. The successful implementation of metal wires or cheap flexible commercial threads as DSC electrodes represents a possibly interesting concept for future wearable solar cells since.²⁹⁵⁻²⁹⁸ Although it is presumably difficult to gauge the PCEs for such shaped miniature devices, a PCE of 7.2% and 8.5% were reported using titanium wire coated with TiO₂ nanoparticles as PE and either platinized StSt wire or graphene/CNT composite fiber with Pt nanoparticles as CE.^{297, 299} PEDOT:PSS-coated flexible commercial carbon fibers and polyester threads were also integrated as CE in fiber-shaped DSCs delivering a PCE of 5.5% and 4.8% respectively.^{295, 296}

12. Conclusions and outlook

We have reviewed flexible dye solar cell (FDSC) technology. Metal based devices permit high temperature processes for more effective charge collection but are limited by issues including partial opacity of electrolytes and corrosion of the cheapest metallic foils. Constraints arising from stability of plastic substrates have brought the development of a surprising breadth of different material

formulations, especially for fabrication of the photo- and counter- electrodes (PEs and CEs), and processing techniques, with results that in a number of cases come close to glass-based devices for both photo- and counter-electrodes. Efficiencies above 8.5% for metal-plastic devices and above 8 % for plastic-plastic devices on small active areas and 5-7% on the active area of larger modules have been reported in standard AM1.5G illumination conditions. Remarkable power outputs, superior than some of the main competing flexible photovoltaic technologies, have been observed in indoor conditions. In fact, the integration and commercial availability of FDSCs in portable or indoor products represents an important endorsement for this technology, which the field has to exploit as a launching pad for continual development in the roadmap of improved performance and market adoption. Roadmaps must consider power output, costs and stability, apart from the peculiar desirable characteristics of easy-integration of thin, lightweight, conformable FDSCs. Thus material combinations with highly stable, transparent (especially for metal PEs), less corrosive (even solid or quasi solid) electrolytes, and stable strongly-absorbing dyes, more resistant to ingress of moisture from the outside, must be developed in parallel to continually more effective solutions for cost-effective transparent, flexible encapsulants and permeation barriers. Maintaining efficiency and performance consistently close to laboratory prototypes over total large-area modules produced in an industrially applicable

manufacturing line is also a challenge including assembling PEs with even higher collection efficiencies on plastic, for example. Reviewing the literature it becomes apparent that not enough works concern the long term stability of FDSCs which needs to improve over continual operation in outdoor environments and thus requires more consistent efforts in order to compete in that arena with inorganic flexible photovoltaics already on the market. Furthermore FDSCs compete with new generation technologies such as flexible organic³⁰⁰⁻³¹¹ and perovskite^{135, 312, 313} cells which can also represent an opportunity for cross-fertilization for future hybrid devices. Finally, recent development of TCO-free architectures, including integrating conducting meshes, monolithic designs and cylindrical and wire shaped devices represent a proof that the technology is fertile ground for new concepts.

Acknowledgements

The authors thank Regione Lazio 'Polo Solare Organico Regione Lazio', the Italian Ministero dell'Istruzione, dell'Università e della Ricerca (MIUR) and the Seventh Framework Program of the EU through the project SINEAD, part of the Eragnet MATERA+ initiative, and MIUR, through the PRIN 2012 (2012A4Z2RY) AQUASOL project, for financial support.

Table and figures

| Morphology / Material | Starting materials/ synthesis | Deposition technique | "Sintering" method | Notes | PCE max [%] | REF |
|--|--|--|--|---|------------------------|-----|
| Mesoporous TiO ₂ | Degussa P25 | Screen Printing | Thermal (100°C) | | 0.25 | 102 |
| Mesoporous PMMA/TiO ₂ | Hydrothermal synthesis | Blocking layer spin coating + Doctor Blade | 80 Mpa @120°C | Enhanced resistance to pre-bending r=10 mm | 3.3 | 88 |
| Mesoporous TiO ₂ nanotube | Degussa P25 + TTIP | Doctor Blade | UV-O ₃ + TTIP chemical sintering | Pre-heating | 3.3 | 70 |
| Mesoporous TiO ₂ | Degussa P25 | Spray | UV assisted | Excimer laser annealing | 3.3 | 121 |
| Mesoporous TiO ₂ | Degussa P25 + Titanium ammonium lactate | Ink-jet | UV assisted | | 3.4 | 99 |
| Mesoporous TiO ₂ | Showa F-5 (20-30nm) | Electrophoretic Deposition | UV assisted CVD | | 3.8 | 126 |
| Mesoporous Double walled CNTs/TiO ₂ | Degussa P25 + TiO ₂ -Double Walled CNTs | Doctor blade | UV assisted | UV decomposition of polyvinylpyrrolidone binder | 3.9 | 87 |
| Mesoporous ZnO | 20 nm from Uni-Onward | Electrophoretic Deposition | 100 MPa Compression + UV treatment | UV pretreatment on ITO/PET | 4.0 | 91 |
| Mesoporous TiO ₂ | Pre-sintered Degussa P25 | Vacuum cold spray | As Deposited | TiCl ₄ on presintered P25 | 4.2 | 82 |
| Mesoporous TiO ₂ | Solvothermal synthesis | Doctor Blade | Thermal (150°C) | Urchin like microsphere Quasi-solid state | 4.3 | 81 |
| Mesoporous TiO ₂ | Degussa P25 | Doctor Blade | UV assisted | UV decomposition of cellulose binder | 4.3 | 116 |
| Mesoporous TiO ₂ | Degussa P25 | Electrophoretic Deposition | 100 mPa Compression | Integrated supercapacitor | 4.4 | 314 |
| Mesoporous TiO ₂ | Degussa P25 | Doctor Blade | Compression | N719/black dye | 4.6 | 149 |
| Mesoporous TiO ₂ | Degussa P25 | Doctor Blade | a) Static Compression b) Continuous compression | Roller mill press | a) 4.6 b) 3.4 | 108 |

| | | | | | | |
|--|---|--|--|--|----------------|-----|
| Mesoporous TiO ₂ | Degussa P25 | a) Gravure printing b) Doctor Blade | 100 MPa Calender press 10 m/min | Calender press | a)1.7 b)4.7 | 98 |
| Mesoporous TiO ₂ | Degussa P25 | Doctor Blade | Thermal (150°C) + HCl chemical sintering | Enhanced adhesion | 5 | 66 |
| Mesoporous TiO ₂ | TiO ₂ nanowire + Degussa P25 | Transfer | Doctor blade + transfer + compression | TiCl ₄ on nanowire | 5.5 | 86 |
| Mesoporous TiO ₂ | Degussa P25 | Spray + Friction transfer | Thermal + transfer + Compression + Chemical | Chemical bath in Titanium butoxide solution | 5.7 | 107 |
| Mesoporous TiO ₂ | Showa Denko F5 (20 nm) | Doctor blade / Screen printing | Thermal (150°C)/chemical with brookite sol | Highly viscous water/t-butanol binder free paste | 5.8 | 75 |
| Mesoporous TiO ₂ | Hydrothermal synthesis | Doctor Blade | Chemical sintering | TiO ₂ Nanoparticle glue | 5.8 | 315 |
| Mesoporous TiO ₂ | Hydrothermal synthesis | Ink-jet + transfer | Thermal + transfer + Compression | | 5.8 | 104 |
| Mesoporous TiO ₂ | Degussa P25 | Electrospray | Compression + TTB treatment | Hierarchical structure | 5.6 | 127 |
| Mesoporous TiO ₂ | Degussa P25 | Doctor Blade | 200 MPa Cold isostatic pressing | transparent | 6.3 | 72 |
| Mesoporous MgO coated SnO ₂ | MgO coated SnO ₂ | Electrophoretic Deposition | 150 MPa Compression | High J _{sc} = 18 mA cm ⁻¹ | 6.5 | 92 |
| Mesoporous TiO ₂ | Degussa P25 + scattering TiO ₂ (7:3) | Doctor Blade | 100 MPa Compression | Hybrid electrolyte | 6.5 | 78 |
| Mesoporous TiO ₂ | Degussa P25 | Doctor blade + spin coating + Transfer | Transfer + compression | 2 dyes | 6.6 | 105 |
| Mesoporous TiO ₂ | Degussa P90 | Electrophoretic Deposition | Compression | | 6.6 | 103 |
| Mesoporous TiO ₂ | Presintered Degussa P25 | Doctor Blade | UV assisted + water 100°C | Sb,In-SnO ₂ nanoglu | 6.8 | 90 |
| Mesoporous TiO ₂ | Hydrothermal synthesis | Doctor Blade | 100 MPa Compression | 20 and 100 nm particles (7:3) Photoplatinization | 7.0 | 110 |
| Mesoporous TiO ₂ | Solvothermal synthesis + CCIC 18 nm | Doctor Blade | 100 MPa Cold isostatic pressing | Mesobead + 18 nm CCIC | 7.5 | 83 |
| Mesoporous TiO ₂ | Hydrothermal synthesis | Doctor Blade | 100 MPa Compression | 20 and 100 nm particles (7:3) | 8.1 | 74 |

Table 1. Examples of different film morphology, material, deposition and processing techniques used for fabrication of fully flexible DSCs with

photoelectrodes on plastic substrates and the power conversion efficiencies (PCEs) of devices fabricated with these plastic-based PEs.

| Morphology / Material | Starting materials/ synthesis | Deposition technique | "Sintering" method | Notes | PCE max [%] | REF |
|---|----------------------------------|--|-------------------------------|---|------------------|-----|
| Nanotubes on Ti foil | Ti foil | Ti foil etching | | N945 dye | 3.6 | 146 |
| Mesoporous TiO ₂ | Hydrothermal synthesis | Screen Printing | Thermal (500°C) | TCO free back-contact monolithical | 4.2 | 292 |
| Nanoparticles on Nanotubes | Hydrothermal synthesis | a) Ti foil etching + Electrophoretic Deposition b) Electrophoretic Deposition | Thermal (500°C) | Ti foil polishing | a) 6.3 b) 4.3 | 316 |
| Mesoporous TiO ₂ on Ti foil | a) Degussa P90 b) Degussa P25 | EPD | Compression + Thermal (350°C) | | a) 6.5 b) 5.2 | 140 |
| Nanoparticles on Nanotubes | Ishihara ST-21 | a) Ti foil etching + Doctor blade b) Doctor blade | Thermal (450°C) | Ti foil polishing | a) 6.7 b) 5.6 | 317 |
| Mesoporous TiO ₂ on Ti foil | Hydrothermal synthesis | | Thermal (high T) | NREL certified (2005) | 7.17 | 139 |
| Mesoporous on Ti foil | Hydrothermal synthesis | Screen Printing | Thermal (500°C) | H ₂ O ₂ pretreatment SiO ₂ beads | 7.2 | 145 |
| Mesoporous on Ti foil | Hydrothermal synthesis | Screen Printing | Thermal (500°C) | TiCl ₄ pretreatment | 7.2 | 142 |
| Mesoporous on Ti foil | Hydrothermal synthesis | Screen Printing | Thermal (500°C) | HF pretreatment | 8.1 | 110 |
| Mesoporous TiO ₂ on Ti foil | Solaronix Nanoxide D/SP | Screen printing | Thermal (500°C) | acid + H ₂ O ₂ + TiCl ₄ Ti foil pretreatment | 8.5 | 144 |
| Mesoporous on StS+SiO _x +ITO | Hydrothermal synthesis | Doctor Blade | Thermal (600°C) | Record for flexible DSC | 8.6 | 73 |

Table 2: Examples of different film morphology, material, deposition and processing techniques used for fabrication of fully flexible DSCs with photoelectrodes all based on TiO₂ on metal foils and the power conversion efficiencies (PCEs) of devices fabricated with these metal-based PEs.

| method | CE catalyst/ substrate | redox mediat or | R_{ct} | optical transmittance | PCE | Ref. |
|-------------------------------------|--|-----------------------|--|--------------------------|--|-------|
| Sputtering | Pt / Ti | I/I_3^- | ----- | opaque | 7.6% (1.111 cm ²) | [74] |
| | Pt / ITOPEN | I/I_3^- | ----- | ----- | 8.1% (0.25 cm ²) | |
| | Pt / ITOPEN | I/I_3^- | 10.35 Ω -cm ² | \approx 70% | 4.33% (deposition time 30 s) 5.95% (with optimized TiO ₂ and electrolyte) | [171] |
| Spray coating | Pt/SWCNT / ITOPEN | I/I_3^- | 1.62 Ω -cm ² | 74-81% | 5.96% | [183] |
| | Pt / ITOPEN | I/I_3^- | ----- | Transparent | 8.5% | [144] |
| Spin coating | Pt/PANI / ITOPET | I/I_3^- | 1.12 Ω -cm ² | 70% (at 480 nm) | 5.4% (front) 4.0% (back) | [318] |
| Chemical reduction | Pt / ITOPEN | I/I_3^- | 0.26 – 1.38 Ω -cm ² | 70% | 5.41% | [154] |
| Electrochemi cal deposition | Pt / ITOPEN | I/I_3^- | 31 Ω | 90% | 7.2% | [142] |
| | Pt / ITOPEN | I/I_3^- | \approx 2 Ω -cm ² | >75% | 6.53 \pm 0.45% | [319] |
| | PProDOT / ITOPEN | I/I_3^- | ----- | ----- | 5.2% | [161] |
| | Pt / Ti mesh | I/I_3^- | 49.6 Ω -cm ² | 92.31% (calculated) | 6.13% (80 cm ² , outdoor natural light 55 mW/cm ²) | [198] |
| | PEDOT / Ti mesh | I/I_3^- | 34.4 Ω -cm ² | 92.31% (calculated) | 6.33% (100 cm ² , outdoor natural light 55 mW/cm ²) | [199] |
| Electrophore tic deposition | Pt / ITOPEN | I/I_3^- | 2.16 Ω -cm ² | 72% (at 500 nm) | 5.8% | [320] |
| Solid-state polymerizati on | PEDOT / plastic substrate | I/I_3^- | 1.33 Ω -cm ² | ----- | 4.65% (full plastic DSC) | [160] |
| Atomic layer deposition | Pt / ITOPEN | I/I_3^- | \approx 10 Ω -cm ² | >90% | 3.71% (0.25 cm ²) 3.10% (17.6 cm ²) | [153] |
| Printing | TiO ₂ -ITO / PEDOT- PSS / ITOPEN | I/I_3^- | ----- | Semi- transparent | 4.38% | [185] |
| | TiC - functionaliz ed CC / PI | I/I_3^- (gel) | 1.67 Ω -cm ² | opaque | 4.26% | [167] |
| Photoreducti on under UV / UV | Pt / tetra-n- butyl titanate- modified | I/I_3^- | 0.66 Ω -cm ² | 76.5% | 8.12% (Ti foil PE) 6.97% (plastic PE, front) 6.26% (plastic, back) | [110] |

| | | | | | | |
|-------------|------------|-------------------------------|---------------------|-------|--|--------------------|
| irradiation | ITOPEN | | | | | |
| | Pt / ITOPE | I/I ₃ ⁻ | 3 Ω·cm ² | ----- | 4.3% (100 mW/cm ²) 5.0% (18 mW/cm ²) 2.3% (100 mW/cm ² , W-type module) | [¹¹⁶] |

Table 3 Examples of published catalyst materials on different flexible substrate and redox mediators, sorted by fabrication/deposition method. Charge transfer resistance at catalyst/electrolyte interface, optical transmittance and power conversion efficiency (PCE) are reported in devices where even the PE was on flexible foil or film (in **all**-flexible DSCs).

| Iodine and iodine salt | Additives | Solvent | Gelificator | Deposition technique | Photoelectrode | PCE max [%] | Stability respect to max PCE | REF |
|---|--|---|--|--------------------------------|--|------------------|----------------------------------|----------------|
| DMPII 0.6 M ^a LiI 0.1 M I ₂ 0.05M | 4-TBP 0.5 M ^b | ACN ^c | None | Backvacuum filling | Compressed TiO ₂ on PET/ITO | 8.2 | Not tested | ⁷⁴ |
| PMII 0.6 M ^d LiI 0.06 M I ₂ 0.03 M | GuSCN 0.1 M ^e 4-TBP 0.5 M ^b | ACN ^c | None | Backvacuum filling | Sintered TiO ₂ on Ti foil | 8.5 | Not tested | ¹⁴⁴ |
| BMI 0.6 M ^f I ₂ 0.03 M | GuSCN 0.1 M ^e 4-TBP 0.5 M ^b | ACN ^c / VLN ^g (85:15) | None | Backvacuum filling | Sintered TiO ₂ on StS/SiO ₂ /ITO | 8.6 | Not tested | ⁷³ |
| LiI 0.5 M I ₂ 0.05M | 4-TBP 0.05 M ^b | ACN ^c | PVdF-HFP/P123 ^j | Transfer of dipped membrane | Compressed TiO ₂ on PET/ITO | 3 | Enhanced | ²¹⁴ |
| PMII 2 M ^d | none | GBL ^h | PEGlyated polymer | "applied on TiO ₂ " | Low temperature sintered TiO ₂ on PET/ITO | 4.3 | Not tested | ¹⁴⁸ |
| a)PMII 0.8 M ^d I ₂ 0.04 M b)PMII 0.8 M ^d I ₂ 0.1 M | a) 4-TBP 0.5 M ^b b) 4-TBP 0.5 M ^b | a) ACN ^c b) MPN ⁱ | 500 nm SiO ₂ | Backvacuum filling | Sintered TiO ₂ on Ti foil (module) | a) 7.1 b) 5.4 | b) >80% after 1500h 1sun @ 50 °C | ¹⁴⁵ |
| DMPII 0.8 M ^a I ₂ 0.1 M | NMB 0.45 M ^k | MPN ⁱ | a) 17.5% TiO ₂ (P25) b) none | Backvacuum filling | Compressed TiO ₂ on PET/ITO | 6.5 5.9 | 81% after 500h 1sun @ 60°C | ⁷⁸ |
| I ₂ 0.2 M | NMB 0.5 M ^k GuSCN 0.1 ^e | 65% PMII ^d 35% EMITC B ^m | a) 17.5% TiO ₂ (P25) b) none | Backvacuum filling | Compressed TiO ₂ on PET/ITO | 2.8 1.6 | 97% after 500h 1sun @ 50°C | ⁷⁸ |
| TBAI 0.4 M ^l I ₂ 0.02 M | NMB 0.3 M ^k | MPN ⁱ /ACN ^c (1:1) | Mesoporous silica nanoparticles 10% + SiO ₂ nanoparticles | "Spreading/injection" | Low temperature sintered TiO ₂ on PET/ITO | 5.5 | Not tested | ²¹⁹ |

| | | | 6% | | | | | |
|--|--|---|------|-----------------------|---|----------------------------|---|---------------|
| I ₂ 0.04 M LiI 0.04 M TBAI 0.4 M ^l | a) 4-TBP 0.3 M ^b b) NMB 0.3 M ^k c) NMB 0.3 M ^k | a) MPN _i b) MPN _i c) MPN _i / ACN _c (1:1) | None | Backvacuum filling | Low temperatur e sintered TiO ₂ on PET ITO | a) 4.6 b) 4.9 c) 5.5 | Outdoor Test of series- connecte d module | ⁷⁵ |
| a) I ₂ 0.04 M LiI 0.04 M TBAI 0.4 M ^l b) TBAI 0.8 M ^l I ₂ 0.2 M c) PMII 0.8M ^d | NMB 0.5 M ^k | a) MPN _i / ACN _c (1:1) b) MPN _i c) MPN _i | None | Backvacuum filling | Compresse d TiO ₂ on PET/ITO | a) 6 b) 3.2 c) 2.3 | a) ITO degradati on b) 75 % 1000h 1sun@ 60°C c) 65 % 1000h 1sun@ 60°C | ⁶⁷ |

Table 4: Summary of different electrolyte formulations used for fabrication of fully flexible DSCs.

| <i>Module type</i> | <i>Photoelectrode</i> | <i>Counterelectrode</i> | <i>Size (cm²)</i> | <i>Efficiency (%)</i> | <i>Ref.</i> |
|--------------------|--|--------------------------------|------------------------------|-----------------------|-------------|
| Parallel | Low-T pressed TiO ₂ on ITO-PEN | Pt sputtered on ITO-PEN | 69.2 (act) | 4.5 | 231 |
| | High-T TiO ₂ NP on Ti foil | Pt ALD on ITO-PEN | 17.6 (act) | 3 | 153 |
| | High-T TiO ₂ NP ITO-SiO _x -StSt foil | Pt chemical reduced on ITO-PET | 51.8 (act) | 3 | 237 |
| | High-T TiO ₂ NT on Ti foil | Pt ALD on ITO-PEN | 5.4 (act) | 4.77 | 235 |
| | High-T TiO ₂ NT on Ti foil | Pt ALD on ITO-PEN | 22.1 (act) | 7.13 | 236 |
| Series Z | Low-T TiO ₂ on ITO- PEN | Sputtered Ti/Pt on ITO-PEN | NA | 2 * | 27 |
| Series Z | High-T TiO ₂ NP on Ti foil | Sputtered Pt on ITO-PEN | >200 (act) | 4.97 % | 139 |

| | | | | | |
|---------------------------------|---|---|------------|---------------|-----|
| Series W | UV processed TiO ₂ on ITO/PEN | UV processed Pt on ITO/PEN | 16.4 (act) | 2.3 | 116 |
| Single cell (large area) | High-T TiO ₂ NP on Ti foil | PEDOT–Pt/Ti mesh | 100 (act) | 6.7 ** | 143 |
| | Hydrothermal TiO ₂ NW on Ti foil | Low-T vacuum decomposition of Pt-SWCNT on Ti mesh | 100 (act) | 6.43** | 239 |

* Efficiency was measured at 0.3 sun

** Efficiency was measured at 0.55 sun in outdoor conditions

Table 5: data on flexible dye solar cell modules, for different types of architectures specifying also the photoelectrode and counterelectrode composition, the size (active area (ac) or aperture area (ap)) and the power conversion efficiency (PCE) in standard measurement 1 sun conditions unless specified.

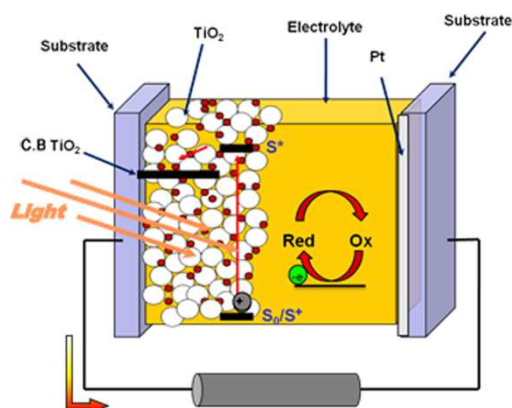


Figure 1. Schematics of the basic operation of a dye solar cell (DSC) consisting in its simplest form of two conducting substrates. On the left is the electron collecting electrode (photoelectrode, PE) covered by a mesoporous TiO₂ layer, sensitized by a monolayer of dye molecules. Light excites the molecule (S*). The electron is injected into the conduction band (C.B.) of the TiO₂ where it diffuses to the transparent contact. After flowing through the load, the electron is shuttled towards the dye (which reverts back to its ground state S₀) via ions in the electrolyte. The catalyst layer of the counterelectrode (Pt in this embodiment) enables the effective reduction of the ionic species of the Red-Ox couple and thus a quick passage of charges between the electrode and the electrolyte.

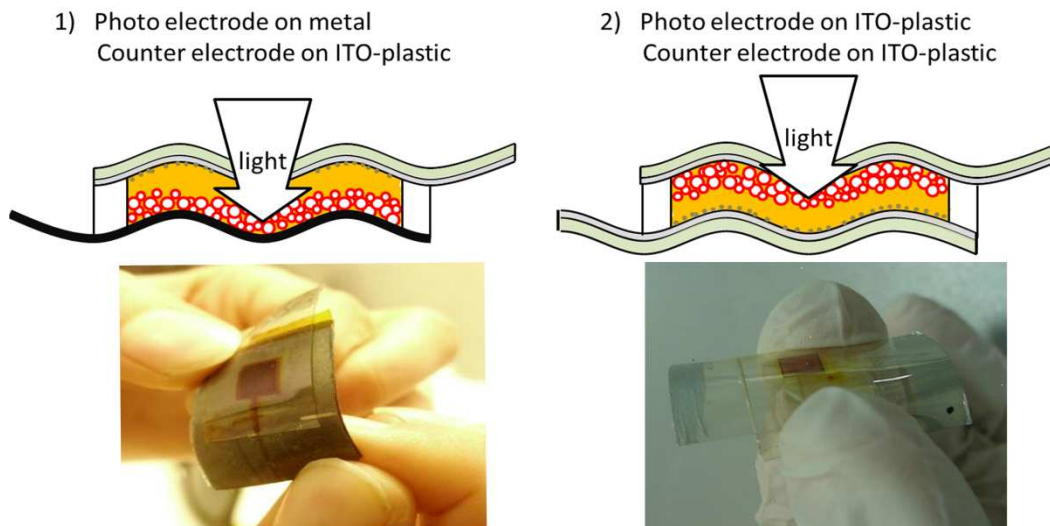


Figure 2. Main sandwich-type architectures (above) for flexible dye solar cells (FDSCs) and associated photographs (CHOSE laboratories) of such devices (below). a) FDSC with bottom metal substrate as photoelectrode and top conductive plastic as counterelectrode through which light is incident and partially absorbed by the electrolyte chamber before reaching the dye sensitized layer; b) FDSC with both substrates being conductive plastic films. In (b) light is shone through the (top) photoelectrode. Another type of device consists of a metal substrate as the counterelectrode and a conductive plastic film as the photoelectrode (not shown).

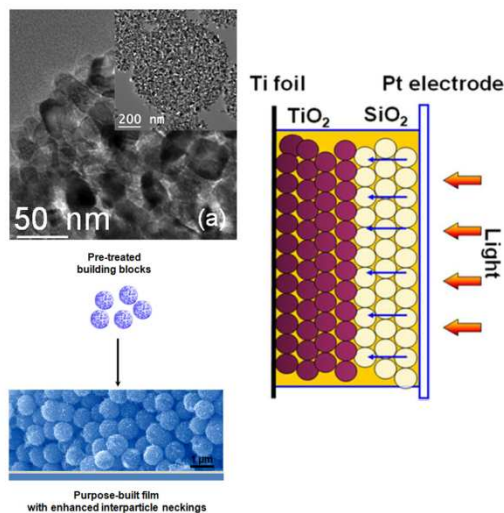


Figure 3: (left) schematic representation of the fabrication of a mesoporous TiO_2 photoelectrode (bottom) starting from pre-formed mesoporous beads building blocks (diameters $> 100\text{nm}$, SEM image (top)) devised to improve overall charge transport compared to smaller less well-connected nanoparticle powders (10-25nm diameters) typically employed for fabrication of the PE of DSCs⁸³. (right) illustration of a FDSC with a Ti photoelectrode (PE) where light has to be incident through the counterelectrode. A SiO_2 mesoporous layer (white circles) was incorporated over the TiO_2 layer (purple circles) so as to decrease the volume occupied by the electrolyte increasing its transparency and thus improving light harvesting at the PE.²³⁶ Figures reproduced with permission from (left) ref.⁸³, © 2013, AIP Publishing LLC, and (right) ref.²³⁶ © 2013 RSC.

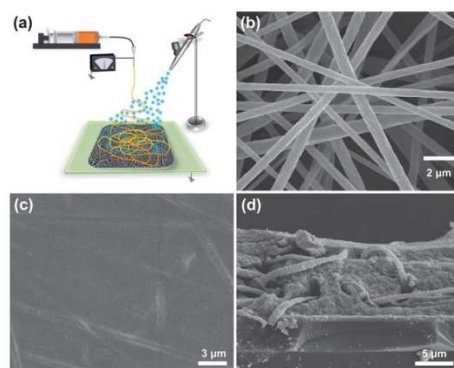


Figure 4: (a) schematic representation of the combined electro-spray/electro-spinning deposition of the TiO_2/PVDF composite photoanode. SEM images of (b) as-spun PVDF nanofibers, (c) top view of as-prepared PVDF/ TiO_2 composite layer, and (d) cross section of a compressed PVDF/ TiO_2 composite film showing enhanced resistance to bending.⁸⁹ Figure reproduced with permission from ref. ⁸⁹ © 2012 RSC.

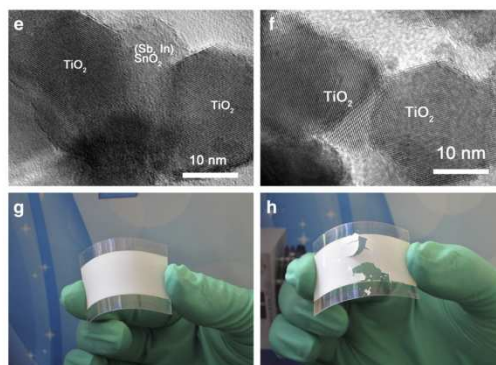


Figure 5: TEM images of TiO₂ photoanode e) with (Sb,In)-doped SnO₂ interconnecting particles and f) without interconnecting agent. Photographs showing different mechanical properties to bending of the TiO₂ films g) with (Sb,In)-doped SnO₂ interconnecting particles and h) without interconnecting agent.⁹⁰ Figure reproduced with permission from ref.⁹⁰ © 2013 Elsevier.

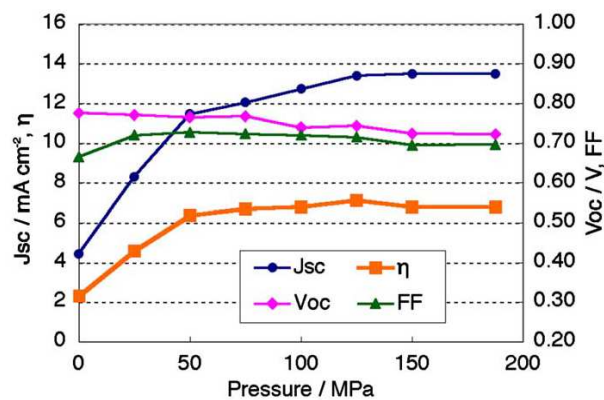


Figure 6: Photovoltaic parameters of a fully plastic DSC as a function of the pressure applied on the TiO_2 film with a hydraulic press for one minute at room temperature⁷⁴. Figure reproduced with permission from ref. ⁷⁴ © 2010 Elsevier.

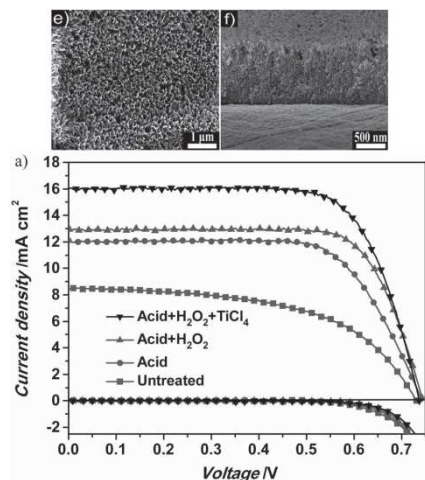


Figure 7: (top images) Surface (e) and cross-sectional (f) SEM images of Ti substrates after acid + H₂O₂ + TiCl₄ treatment. (bottom image) JV curves of FDSCs fabricated on Ti substrates which previously underwent different treatments. The acid + H₂O₂ + TiCl₄ process led to the cells with the highest photocurrents.¹⁴⁴ Figure reproduced with permission from ref. ¹⁴⁴ © 2012 John Wiley and Sons

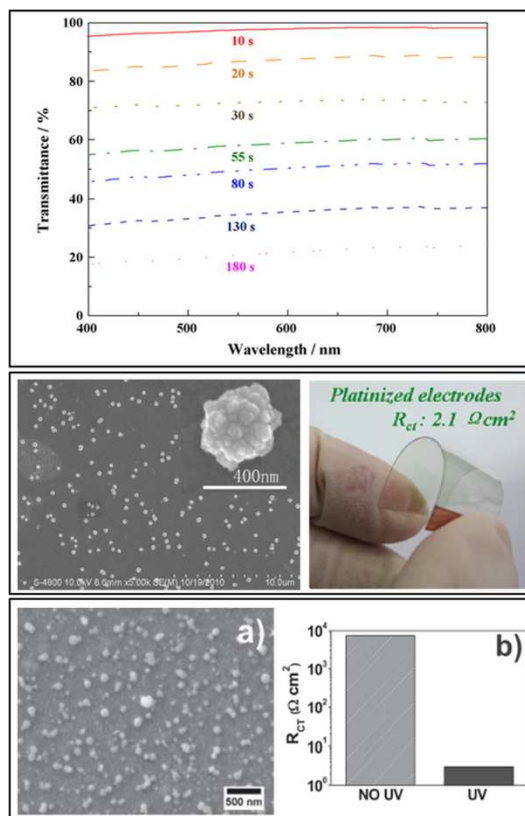


Fig. 8: Platinized electrodes on ITO plastic substrates. (top) transmittance spectra of sputtered Pt for different deposition times (baseline with bare ITO electrode)¹⁷¹; (middle) SEM image of electrodeposited Pt and a picture showing the plastic CE with over 75% transparency and high bendability³¹⁹; (bottom) SEM image of printed Pt after UV irradiation and the dramatic change in its R_{ct} before and after UV treatment¹¹⁶. Figures reproduced with permission from: (top) ref ¹⁷¹ © 2010 Elsevier; (middle) ref ³¹⁹ © 2012 ACS; (bottom) ref ¹¹⁶ © 2013 John Wiley and Sons.

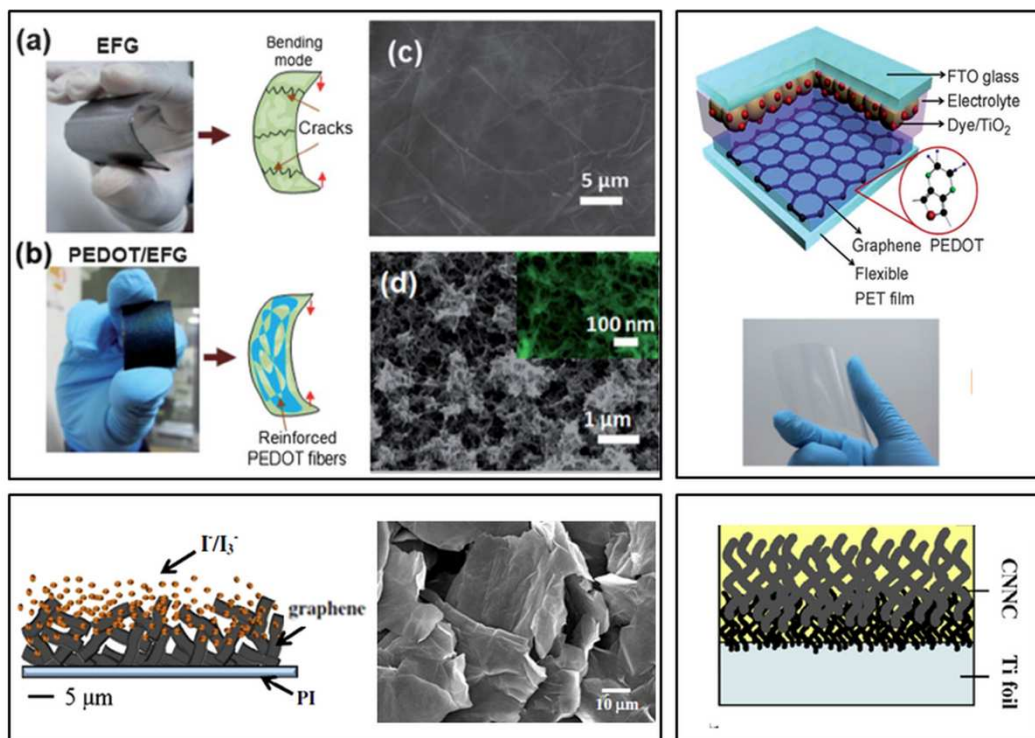


Fig. 9: ITO-free CEs on flexible substrates. (top, left) pictures, schematics and SEM images of exfoliated graphite (EFG) substrate and of electropolymerized PEDOT on EFG, showing the added value of the polymer in increasing substrate bendability¹⁹¹. (top, right) spin-coated PEDOT on graphene/PET substrate reaching over 70% transparency¹⁹³. (bottom, left) schematics and SEM image of freeze-dried reduced graphene oxide on polyimide (PI), showing the porous structure with several edges, responsible for highly catalytic activity¹⁹⁰. (bottom, right) schematics of hierarchical porous nano-carbon CEs on Ti foil²⁰⁰, CNNC = carbon nanotubes (more compact) and carbon nanofibers (porous) composite. Figures reproduced with permission from: (top, left) ref¹⁹¹© 2014 RSC; (top, right) ref¹⁹³ © 2012 John Wiley and Sons; (bottom, left) ref¹⁹⁰ © 2013 Elsevier; (bottom, right) ref²⁰⁰ © 2012 Elsevier.

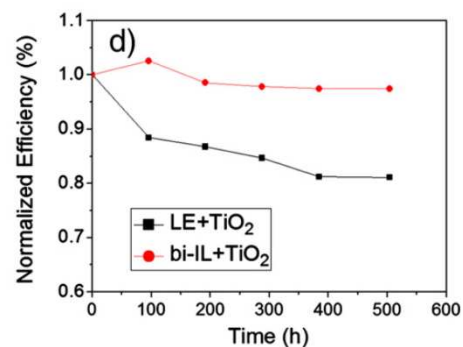


Figure 10: Normalized efficiency of a plastic dye solar cell during a light soaking ageing test at 1 Sun and 60°C assembled with different electrolytes showing the considerable bearing of electrolytes on the lifetime of FDSCs: bi-EL is a binary ionic gellified electrolyte with 17.5% of TiO₂ Degussa P25, while LE-EL is a gel electrolyte made by adding 17.5% of TiO₂ Degussa P25 to a methoxypropionitrile based formulation.⁷⁸ Figure reproduced with permission from ref. ⁷⁸ © 2013 Elsevier.

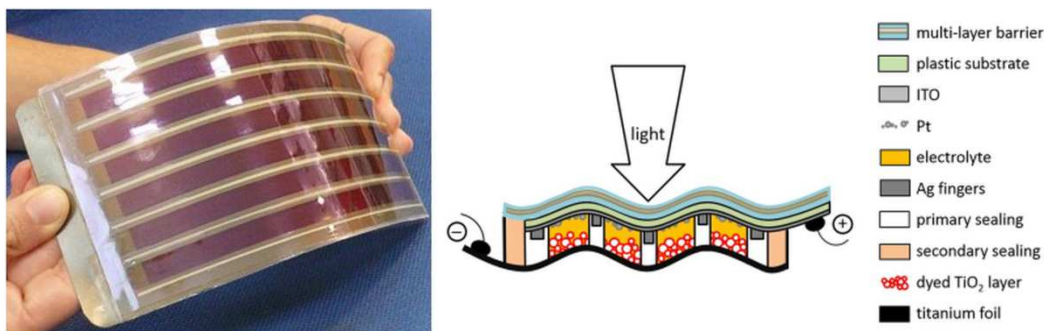


Figure. 11. (left image) A photograph of metal/plastic parallel module (CHOSE laboratories). (right image) cross section a parallel Ti/plastic-CE module with: conductive Ag collecting grids for current collection; primary sealing which protects the grids from electrolyte corrosion, seals the two electrodes together and avoids egress of electrolyte; secondary sealing applied at the perimeter for improved bonding and to minimize ingress of oxygen and water vapour; multilayer ultra-high barrier film applied over the plastic electrode to minimize gas permeation rates. Combined encapsulation and barrier strategies like these, in tandem with stable active material combinations, are developed to increase lifetimes.

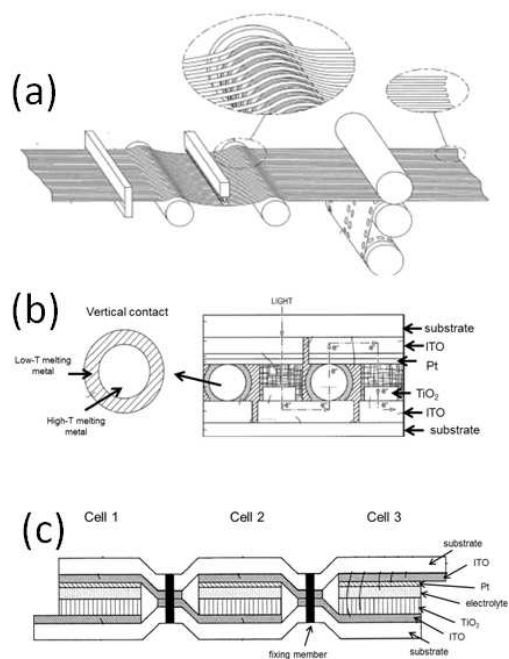


Figure 12. (a) Schematics of the R-2.R process for fabrication of FDSCs disclosed in ref.²⁴⁵. A rolling metallic substrate on which a plurality of TiO₂ films strips has been previously printed is cut in order to separate single photoelectrodes and successively separated for subsequent manufacturing steps. (b) A method to contact cells utilising a metal with high melting temperature core coated with a low T melting metal²⁴⁶. (c) Schematics of a method for series connection utilizing a fixing member²⁴⁷.

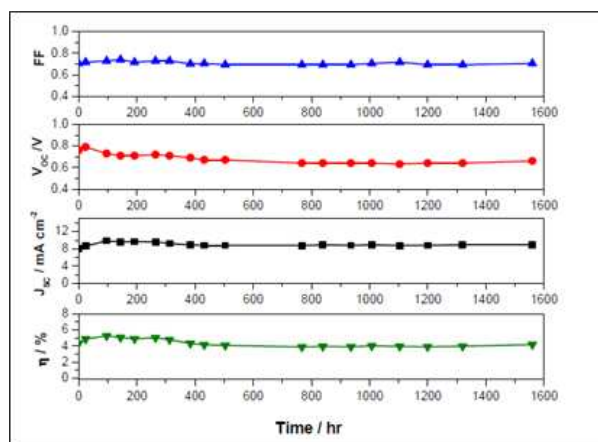


Figure 13. Photovoltaic parameters (FF, V_{oc} , J_{sc} and efficiency η) extracted from a large area FDSC sub module during a 1600 h ageing test. The submodule was exposed under a light soaker ($1000 \text{ W}\cdot\text{m}^{-2}$) at $T=50 \text{ }^\circ\text{C}$.²³⁶ Figure reproduced with permission from ref.²³⁶ © 2013 RSC.



Figure 14. Current and envisaged future products integrating (flexible and rigid) DSCs²⁸⁷. The current main sector of application is in indoor, portable and disposable electronics but DSCs are forecasted to penetrate in several market segments in the next few years, including BIPV, depending on opportunities, technical developments and competition. Figure reproduced with permission from ref. ²⁸⁷ © IDTechEx.

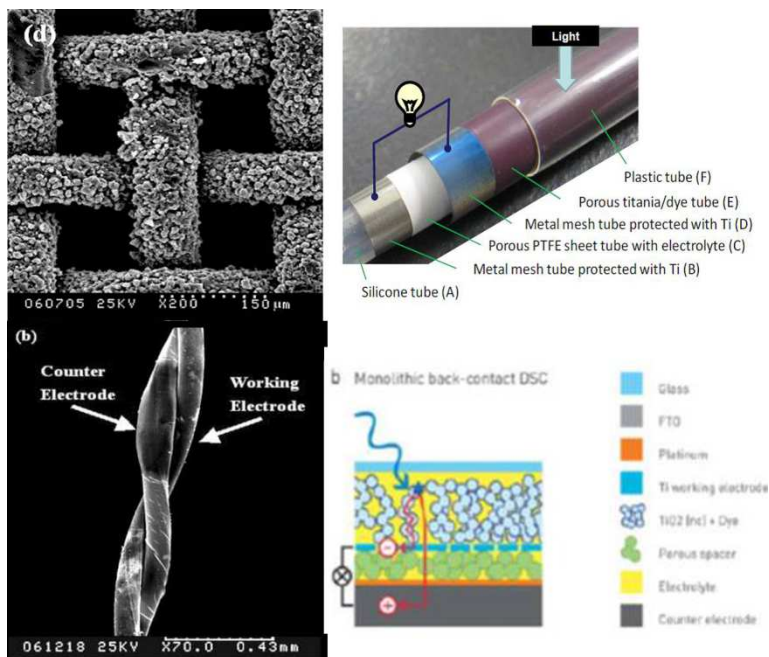


Figure 15. (Top left) SEM photos of the metallic mesh coated with porous TiO₂ layer to be used as a TCO-free photoelectrode.⁵⁴ (Top right) Cylindrical transparent TCO-free FDSC consisting of plastic tube/stainless steel mesh–TiO₂–dye/gel electrolytes/Pt-Ti rod.³²¹ (bottom left) SEM image of a flexible device in which two wires, CE and PE, are intertwined to form a DSC.²⁹⁴ (Bottom right) A TCO-free monolithic dye solar cell consisting of two coplanar charge-collecting electrodes. Pt was deposited on the bottom electrode and a titanium working electrode was deposited over a porous ZrO₂ spacer layer. The dye sensitized layer was applied over the stack. The top substrate was a plastic transparent insulating film for a flexible cell and required for electrolyte/device encapsulation²⁹². Figures reproduced with permission from: (top, left) ref.⁵⁴ © 2007 AIP Publishing LLC; (top, right) ref.³²¹ © 2013 OSA; (bottom, left) ref.²⁹⁴ © 2008 John Wiley and Sons; (bottom, right) ref.²⁹² © 2013 RSC.

References

1. B. O'Regan and M. Grätzel, *Nature*, 1991, 353, 737-740.
2. M. Grätzel, *Journal of Photochemistry and Photobiology C: Photochemistry Reviews*, 2003, 4, 145-153.
3. A. Hagfeldt, G. Boschloo, L. Sun, L. Kloo and H. Pettersson, *Chemical reviews*, 2010, 110, 6595-6663.
4. S. K. Balasingam, M. G. Kang and Y. Jun, *Chemical Communications*, 2013, 49, 11457-11475.
5. A. Hagfeldt, G. Boschloo, H. Lindström, E. Figgemeier, A. Holmberg, V. Aranyos, E. Magnusson and L. Malmqvist, *Coordination chemistry reviews*, 2004, 248, 1501-1509.
6. G. Hashmi, K. Miettunen, T. Peltola, J. Halme, I. Asghar, K. Aitola, M. Toivola and P. Lund, *Renewable and Sustainable Energy Reviews*, 2011, 15, 3717-3732.
7. K. Miettunen, J. Halme and P. Lund, *Wiley Interdisciplinary Reviews: Energy and Environment*, 2013, 2, 104-120.
8. M. Toivola, J. Halme, K. Miettunen, K. Aitola and P. D. Lund, *International Journal of Energy Research*, 2009, 33, 1145-1160.
9. M. Grätzel, *Progress in Photovoltaics: Research and Applications*, 2006, 14, 429-442.
10. B. E. Hardin, H. J. Snaith and M. D. McGehee, *Nature Photonics*, 2012, 6, 162-169.
11. A. Listorti, B. O'Regan and J. R. Durrant, *Chemistry of Materials*, 2011, 23, 3381-3399.
12. P. J. Cameron, L. M. Peter and S. Hore, *The Journal of Physical Chemistry B*, 2005, 109, 930-936.
13. F. Lenzmann and J. Kroon, *Advances in OptoElectronics*, 2007, 2007.
14. H. J. Snaith and L. Schmidt-Mende, *Advanced Materials*, 2007, 19, 3187-3200.
15. S. Ito, P. Chen, P. Comte, M. K. Nazeeruddin, P. Liska, P. Péchy and M. Grätzel, *Progress in photovoltaics: research and applications*, 2007, 15, 603-612.
16. M. K. Nazeeruddin, P. Pechy, T. Renouard, S. M. Zakeeruddin, R. Humphry-Baker, P. Comte, P. Liska, L. Cevey, E. Costa and V. Shklover, *Journal of the American Chemical Society*, 2001, 123, 1613-1624.
17. T. N. Murakami and M. Grätzel, *Inorganica Chimica Acta*, 2008, 361, 572-580.

18. M. Wu, X. Lin, Y. Wang, L. Wang, W. Guo, D. Qi, X. Peng, A. Hagfeldt, M. Grätzel and T. Ma, *Journal of the American Chemical Society*, 2012, 134, 3419-3428.
19. M. Wu and T. Ma, *ChemSusChem*, 2012, 5, 1343-1357.
20. F. Giordano, E. Petrolati, T. M. Brown, A. Reale and A. Di Carlo, *Electron Devices, IEEE Transactions on*, 2011, 58, 2759-2764.
21. S. Ito, G. Rothenberger, P. Liska, P. Comte, S. M. Zakeeruddin, P. Péchy, M. K. Nazeeruddin and M. Grätzel, *Chemical Communications*, 2006, 4004-4006.
22. Y. Baojie, Y. Guozhen, J. Yang and S. Guha, *Proc. of the 19th International Workshop on Active-Matrix Flatpanel Displays and Devices (AM-FPD)*, 2012, 67-70.
23. M. A. I. M. M. Aliyu, N. R. Hamzah, M. R. Karim, M. A. Matin, K. Sopian, and N. Amin, *International Journal of Photoenergy*, 2012, 2012.
24. P. Reinhard, A. Chirila, F. Pianezzi, S. Nishiwaki, S. Buecheler and A. N. Tiwari, *Active-Matrix Flatpanel Displays and Devices (AM-FPD), 2013 Twentieth International Workshop on*, 2013, 79-82.
25. W. A. MacDonald, M. K. Looney, D. MacKerron, R. Eveson, R. Adam, K. Hashimoto and K. Rakos, *Journal of the Society for Information Display*, 2007, 15, 1075-1083.
26. V. Zardetto, T. M. Brown, A. Reale and A. Di Carlo, *Journal of Polymer Science Part B: Polymer Physics*, 2011, 49, 638-648.
27. M. Ikegami, J. Suzuki, K. Teshima, M. Kawaraya and T. Miyasaka, *Solar Energy Materials and Solar Cells*, 2009, 93, 836-839.
28. K.-M. Lee, W.-H. Chiu, M.-D. Lu and W.-F. Hsieh, *Journal of Power Sources*, 2011, 196, 8897-8903.
29. K. S. Lee, Y. Lee, J. Y. Lee, J.-H. Ahn and J. H. Park, *ChemSusChem*, 2012, 5, 379-382.
30. K. Aitola, A. Kaskela, J. Halme, V. Ruiz, A. G. Nasibulin, E. I. Kauppinen and P. D. Lund, *Journal of The Electrochemical Society*, 2010, 157, B1831-B1837.
31. K. S. Lee, H. K. Lee, D. H. Wang, N.-G. Park, J. Y. Lee, O. O. Park and J. H. Park, *Chemical Communications*, 2010, 46, 4505-4507.
32. W. He, J. Qiu, F. Zhuge, X. Li, J.-H. Lee, Y.-D. Kim, H.-K. Kim and Y.-H. Hwang, *Nanotechnology*, 2012, 23, 225602.
33. N. Onozawa-Komatsuzaki, K. Sayama, Y. Konishi, H. Sugihara, K. Kawasaki and T. Ebina, *Electrochemistry*, 2011, 79, 801-803.
34. Y.-T. Huang, Y.-Y. Zhan, S.-J. Cherng, C.-M. Chen, S.-P. Feng and T.-C. Wei, *Journal of The Electrochemical Society*, 2013, 160, H581-H586.

35. P. F. Carcia, R. S. McLean, M. H. Reilly, M. D. Groner and S. M. George, *Applied Physics Letters*, 2006, 89, 031915.
36. G. Dennler, C. Lungenschmied, H. Neugebauer, N. S. Sariciftci, M. Latrèche, G. Czeremuszkin and M. R. Wertheimer, *Thin Solid Films*, 2006, 511–512, 349-353.
37. L. T. Huang, M. C. Lin, M. L. Chang, R. R. Wang and H. C. Lin, *Thin Solid Films*, 2009, 517, 4207-4210.
38. K. Teshima, H. Sugimura, Y. Inoue and O. Takai, *Langmuir*, 2003, 19, 8331-8334.
39. G. Aresta, J. Palmans, M. C. M. van de Sanden and M. Creatore, *Journal of Vacuum Science & Technology A: Vacuum, Surfaces, and Films*, 2012, 30, 041503.
40. C.-T. Chou, P.-W. Yu, M.-H. Tseng, C.-C. Hsu, J.-J. Shyue, C.-C. Wang and F.-Y. Tsai, *Advanced Materials*, 2013, 25, 1750-1754.
41. L. Moro, N. M. Rutherford, R. J. Visser, J. A. Hauch, C. Klepek, P. Denk, P. Schilinsky and C. J. Brabec, *Proc. SPIE 6334, Organic Photovoltaics VII*, 2006, 63340M.
42. J. Fahlteich, M. Fahland, W. Schönberger and N. Schiller, *Thin Solid Films*, 2009, 517, 3075-3080.
43. T. Watson, G. Reynolds, D. Wragg, G. Williams and D. Worsley, *International Journal of Photoenergy*, 2013, 2013, 8.
44. K. Miettunen, X. Ruan, T. Saukkonen, J. Halme, M. Toivola, H. Guangsheng and P. Lund, *Journal of The Electrochemical Society*, 2010, 157, B814-B819.
45. T. Ma, X. Fang, M. Akiyama, K. Inoue, H. Noma and E. Abe, *Journal of Electroanalytical Chemistry*, 2004, 574, 77-83.
46. M. Toivola, F. Ahlskog and P. Lund, *Solar Energy Materials and Solar Cells*, 2006, 90, 2881-2893.
47. K. Miettunen, S. Jouttijärvi, R. Jiang, T. Saukkonen, J. Romu, J. Halme and P. Lund, *Journal of The Electrochemical Society*, 2014, 161, H138-H143.
48. K. Miettunen, I. Asghar, X. Ruan, J. Halme, T. Saukkonen and P. Lund, *Journal of Electroanalytical Chemistry*, 2011, 653, 93-99.
49. M.-H. Hong and S.-I. Pyun, *Wear*, 1991, 147, 59-67.
50. N. Vyas, C. Charbonneau, M. Carnie, D. Worsley and T. Watson, *ECS Transactions* 2013, 53 (24), 29-37.
51. A. F. Kanta and A. Decroly, *Electrochimica Acta*, 2011, 56, 10276-10282.
52. W. Kylberg, F. A. de Castro, P. Chabreck, U. Sonderegger, B. T.-T. Chu, F. Nüesch and R. Hany, *Advanced Materials*, 2011, 23, 1015-1019.

53. J. Usakawa, K. Uzaki, T. Kogo, Y. Ogomi, S. Pandey and S. Hayase, *ECS Meeting Abstracts*, 2011, MA2011-02, 193-193.
54. X. Fan, F. Wang, Z. Chu, L. Chen, C. Zhang and D. Zou, *Applied physics letters*, 2007, 90, 073501.
55. J. Usagawa, S. S. Pandey, Y. Ogomi, S. Noguchi, Y. Yamaguchi and S. Hayase, *Progress in Photovoltaics: Research and Applications*, 2013, 21, 517-524.
56. T. Miyasaka, *The Journal of Physical Chemistry Letters*, 2011, 2, 262-269.
57. Y. Xiao, J. Wu, G. Yue, J. Lin, M. Huang, L. Fan and Z. Lan, *Electrochimica Acta*, 2011, 58, 621-627.
58. N. G. Park, J. van de Lagemaat and A. J. Frank, *The Journal of Physical Chemistry B*, 2000, 104, 8989-8994.
59. M. Grätzel, *Chemistry Letters*, 2005, 34, 8-13.
60. S. Nakade, M. Matsuda, S. Kambe, Y. Saito, T. Kitamura, T. Sakata, Y. Wada, H. Mori and S. Yanagida, *The Journal of Physical Chemistry B*, 2002, 106, 10004-10010.
61. S. Ito, T. N. Murakami, P. Comte, P. Liska, C. Grätzel, M. K. Nazeeruddin and M. Grätzel, *Thin Solid Films*, 2008, 516, 4613-4619.
62. S. Agarwala and G. Ho, *Materials Letters*, 2009, 63, 1624-1627.
63. S. Agarwala, M. Kevin, A. Wong, C. Peh, V. Thavasi and G. Ho, *ACS applied materials & interfaces*, 2010, 2, 1844-1850.
64. X. Chen and S. S. Mao, *Chem. Rev.*, 2007, 107, 2891-2959.
65. P. Innocenzi and L. Malfatti, *Chemical Society Reviews*, 2013, 42, 4198-4216.
66. H. C. Weerasinghe, P. M. Sirimanne, G. V. Franks, G. P. Simon and Y. B. Cheng, *Journal of Photochemistry and Photobiology A: Chemistry*, 2010, 213, 30-36.
67. K. M. Lee, W. H. Chiu, M. D. Lu and W. F. Hsieh, *Journal of Power Sources*, 2011, 196, 8897-8903.
68. V. Zardetto, G. De Angelis, L. Vesce, V. Caratto, C. Mazzuca, J. Gasiorowski, A. Reale, A. Di Carlo and T. M. Brown, *Nanotechnology*, 2013, 24, 255401.
69. S. G. Hashmi, J. Halme, T. Saukkonen, E. L. Rautama and P. Lund, *Physical Chemistry Chemical Physics*, 2013, 15, 17689-17695.
70. D. Zhang, T. Yoshida, T. Oekermann, K. Furuta and H. Minoura, *Advanced Functional Materials*, 2006, 16, 1228-1234.
71. S. E. Pratsinis, *Progress in Energy and Combustion Science*, 1998, 24, 197-219.

72. H. C. Weerasinghe, P. M. Sirimanne, G. P. Simon and Y.-B. Cheng, *Progress in Photovoltaics: Research and Applications*, 2012, 20, 321-332.
73. J. H. Park, Y. Jun, H.-G. Yun, S.-Y. Lee and M. G. Kang, *Journal of the Electrochemical Society*, 2008, 155, F145-F149.
74. T. Yamaguchi, N. Tobe, D. Matsumoto, T. Nagai and H. Arakawa, *Solar Energy Materials and Solar Cells*, 2010, 94, 812-816.
75. T. Miyasaka, Y. Kijitori and M. Ikegami, *Electrochemistry*, 2007, 75, 2-12.
76. Y. Li, W. Lee, D.-K. Lee, K. Kim, N.-G. Park and M. J. Ko, *Applied Physics Letters*, 2011, 98, 103301.
77. P. Bosch-Jimenez, Y. Yu, M. Lira-Cantu, C. Domingo and J. A. Ayllón, *Journal of colloid and interface science*, 2014, 416, 112-118.
78. H. F. Lee, Y. T. Chua, S. M. Yang, P. Y. Hsu, F. Y. Ouyang, Y. L. Tung and J. J. Kai, *Thin Solid Films*, 2013, DOI: 10.1016/j.tsf.2013.03.091.
79. Y. Li, K. Yoo, D.-K. Lee, J. Y. Kim, H. Kim, B. Kim and M. J. Ko, *Nanoscale*, 2013, 5, 4711-4719.
80. L. Fan, Y. Chen, J. Wu, Z. Li, Y. Xiao, M. Huang and H. Yu, *Science China Chemistry*, 2013, 56, 1470-1477.
81. K. Fan, T. Peng, J. Chen, X. Zhang and R. Li, *Journal of Power Sources*, 2013, 222, 38-44.
82. G. J. Yang, C. J. Li, K. X. Liao, X. L. He, S. Li and S. Q. Fan, *Thin Solid Films*, 2011, 519, 4709-4713.
83. F. Huang, D. Chen, Q. Li, R. A. Caruso and Y.-B. Cheng, *Applied Physics Letters*, 2012, 100, 123102.
84. L. Vesce, R. Riccitelli, G. Soscia, T. M. Brown, A. Di Carlo and A. Reale, *Journal of Non-Crystalline Solids*, 2010, 356, 1958-1961.
85. S. Q. Fan, C. J. Li, G. J. Yang, J. C. Gao, L. Z. Zhang, C. X. Li and Y. Y. Wang, 2008, vol. 373-374, pp. 742-745.
86. L. Wang, Z. Xue, X. Liu and B. Liu, *RSC Advances*, 2012, 2, 7656-7659.
87. C. Cheng, J. Wu, Y. Xiao, Y. Chen, H. Yu, Z. Tang, J. Lin and M. Huang, *Frontiers of Optoelectronics*, 2012, 5, 224-230.
88. Y. Li, K. Yoo, D. K. Lee, J. H. Kim, N. G. Park, K. Kim and M. J. Ko, *Current Applied Physics*, 2010, 10, e171-e175.
89. Y. Li, D. K. Lee, J. Y. Kim, B. Kim, N. G. Park, K. Kim, J. H. Shin, I. S. Choi and M. J. Ko, *Energy and Environmental Science*, 2012, 5, 8950-8957.
90. N. Q. Fu, Y. D. Duan, Y. Y. Fang, X. W. Zhou, X. R. Xiao and Y. Lin, *Electrochemistry Communications*, 2013, 34, 254-257.

91. H.-W. Chen, C.-Y. Lin, Y.-H. Lai, J.-G. Chen, C.-C. Wang, C.-W. Hu, C.-Y. Hsu, R. Vittal and K.-C. Ho, *Journal of Power Sources*, 2011, 196, 4859-4864.
92. S. Li, Z. Chen, Y. Wang, T. Li, B. Xu and W. Zhang, *Journal of the Electrochemical Society*, 2014, 161, H6-H10.
93. H. Weerasinghe, P. Sirimanne, G. Simon and Y. Cheng, *Journal of Photochemistry and Photobiology A: Chemistry*, 2009, 206, 64-70.
94. H. C. Weerasinghe, G. V. Franks, J. D. Plessis, G. P. Simon and Y.-B. Cheng, *Journal of Materials Chemistry*, 2010, 20, 9954-9961.
95. H. Weerasinghe, P. Sirimanne, G. Franks, G. Simon and Y. Cheng, *Journal of Photochemistry and Photobiology A: Chemistry*, 2010, 213, 30-36.
96. H. C. Weerasinghe, P. M. Sirimanne, G. P. Simon and Y. B. Cheng, *Progress in Photovoltaics: Research and Applications*, 2012, 20, 321-332.
97. F. Pichot, J. R. Pitts and B. A. Gregg, *Langmuir : the ACS journal of surfaces and colloids*, 2000, 16, 5626-5630.
98. H. Santa-Nokki, J. Kallioinen, T. Kololuoma, V. Tuboltsev and J. Korppi-Tommola, *Journal of Photochemistry and Photobiology A: Chemistry*, 2006, 182, 187-191.
99. Y. Oh, S. N. Lee, H. K. Kim and J. Kim, *Journal of the Electrochemical Society*, 2012, 159, H777-H781.
100. H. C. Weerasinghe, F. Huang and Y. B. Cheng, *Nano Energy*, 2013, 2, 174-189.
101. T. Miyasaka and M. Ikegami, *Journal of Photopolymer Science and Technology*, 2010, 23, 269-277.
102. J. E. Hu, S. Y. Yang, J. C. Chou and P. H. Shih, *Micro and Nano Letters*, 2012, 7, 1162-1165.
103. W. H. Chiu, K. M. Lee and W. F. Hsieh, *Journal of Power Sources*, 2011, 196, 3683-3687.
104. M. Dürr, A. Schmid, M. Obermaier, S. Rosselli, A. Yasuda and G. Nelles, *Nature materials*, 2005, 4, 607-611.
105. E. Y. Kim, S. Yu, J. H. Moon, S. M. Yoo, C. Kim, H. K. Kim and W. I. Lee, *Electrochimica Acta*, 2013, 111, 261-267.
106. S. M. Chao, T. H. Meen, Y. T. Jhuo, J. K. Tsai, J. X. Wang, W. R. Chen, T. C. Wu and C. J. Huang, Fuzhou, 2013, vol. 311, pp. 446-450.
107. L. Yang, L. Wu, M. Wu, G. Xin, H. Lin and T. Ma, *Electrochemistry Communications*, 2010, 12, 1000-1003.
108. H. Lindström, A. Holmberg, E. Magnusson, S. E. Lindquist, L. Malmqvist and A. Hagfeldt, *Nano letters*, 2001, 1, 97-100.

109. R. S. Averback, H. J. Höfler, H. Hahn and J. C. Logas, *Nanostructured Materials*, 1992, 1, 173-178.
110. N. Q. Fu, Y. Y. Fang, Y. D. Duan, X. W. Zhou, X. R. Xiao and Y. Lin, *ACS Nano*, 2012, 6, 9596-9605.
111. Y. Peng, J. Z. Liu, K. Wang and Y.-B. Cheng, *International Journal of Photoenergy*, 2011, 2011, 410352.
112. S. Uchida, M. Tomiha, H. Takizawa and M. Kawaraya, *Journal of Photochemistry and Photobiology A: Chemistry*, 2004, 164, 93-96.
113. T. Miyasaka, Y. Kijitori, T. N. Murakami, M. Kimura and S. Uegusa, *Chemistry Letters*, 2002, 31, 1250-1251.
114. R. Thiruvenkatachari, S. Vigneswaran and I. S. Moon, *Korean Journal of Chemical Engineering*, 2008, 25, 64-72.
115. D. Gutiérrez-Tauste, I. Zumeta, E. Vigil, M. A. Hernández-Fenollosa, X. Domènech and J. A. Ayllón, *Journal of Photochemistry and Photobiology A: Chemistry*, 2005, 175, 165-171.
116. V. Zardetto, F. Di Giacomo, D. Garcia-Alonso, W. Keuning, M. Creatore, C. Mazzuca, A. Reale, A. Di Carlo and T. M. Brown, *Advanced Energy Materials*, 2013, 3, 1292-1298.
117. C. Dunsy and F. Colville, *Proc. SPIE*, 2008, 6871, 687129.
118. G. Mincuzzi, M. Schulz-Ruhtenberg, L. Vesce, A. Reale, A. Di Carlo, A. Gillner and T. Brown, *Progress in Photovoltaics: Research and Applications*, 2014, 22, 308-317.
119. G. Mincuzzi, L. Vesce, M. Liberatore, A. Reale, A. Di Carlo and T. M. Brown, *Electron Devices, IEEE Transactions on*, 2011, 58, 3179-3188.
120. G. Mincuzzi, L. Vesce, A. Reale, A. Di Carlo and T. M. Brown, *Applied physics letters*, 2009, 95, 103312.
121. H. Pan, S. H. Ko, N. Misra and C. P. Grigoropoulos, *Applied Physics Letters*, 2009, 94, 071117.
122. J.-W. Lee, J. O. Choi, J.-E. Jeong, S. Yang, S. H. Ahn, K.-W. Kwon and C. S. Lee, *Electrochimica Acta*, 2013, 103, 252-258.
123. L. Ming, H. Yang, W. Zhang, X. Zeng, D. Xiong, Z. Xu, H. Wang, W. Chen, X. Xu, M. Wang, J. Duan, Y.-B. Cheng, J. Zhang, Q. Bao, Z. Wei and S. Yang, *Journal of Materials Chemistry A*, 2014, DOI: 10.1039/C3TA14210H.
124. C. Kim, S. Kim and M. Lee, *Applied Surface Science*, 2013, 270, 462-466.
125. D. Zhang, T. Yoshida, K. Furuta and H. Minoura, *Journal of Photochemistry and Photobiology A: Chemistry*, 2004, 164, 159-166.

126. T. N. Murakami, Y. Kijitori, N. Kawashima and T. Miyasaka, *Journal of Photochemistry and Photobiology A: Chemistry*, 2004, 164, 187-191.
127. H. Lee, D. Hwang, S. M. Jo, D. Kim, Y. Seo and D. Y. Kim, *ACS Applied Materials & Interfaces*, 2012, 4, 3308-3315.
128. P. J. Cameron, L. M. Peter and S. Hore, *The Journal of Physical Chemistry B*, 2004, 109, 930-936.
129. F. Matteocci, G. Mincuzzi, F. Giordano, A. Capasso, E. Artuso, C. Barolo, G. Viscardi, T. M. Brown, A. Reale and A. Di Carlo, *Organic Electronics*, 2013, 14, 1882-1890.
130. L. Yang, U. B. Cappel, E. L. Unger, M. Karlsson, K. M. Karlsson, E. Gabriellsson, L. Sun, G. Boschloo, A. Hagfeldt and E. M. J. Johansson, *Physical Chemistry Chemical Physics*, 2012, 14, 779-789.
131. P. Chen, Y.-W. Lo, T.-L. Chou and J.-M. Ting, *Journal of the Electrochemical Society*, 2011, 158, H1252-H1257.
132. C. Y. Jiang, W. L. Koh, M. Y. Leung, S. Y. Chiam, J. S. Wu and J. Zhang, *Applied Physics Letters*, 2012, 100, 113901.
133. Z. Xue, C. Jiang, L. Wang, W. Liu and B. Liu, *The Journal of Physical Chemistry C*, 2013, DOI: 10.1021/jp408663d.
134. M. H. Kumar, N. Yantara, S. Dharani, M. Graetzel, S. Mhaisalkar, P. P. Boix and N. Mathews, *Chemical Communications*, 2013, 49, 11089-11091.
135. D. Liu and T. L. Kelly, *Nature Photonics*, 2014, 8, 133-138.
136. K. Wojciechowski, M. Saliba, T. Leijtens, A. Abate and H. Snaith, *Energy & Environmental Science*, 2014, 7, 1142-1147.
137. J. T.-W. Wang, J. M. Ball, E. M. Barea, A. Abate, J. A. Alexander-Webber, J. Huang, M. Saliba, I. Mora-Sero, J. Bisquert and H. J. Snaith, *Nano letters*, 2014, 14, 724-730.
138. www.gcell.com.
139. K. G. Chittibabu, 2014, Konarka/G24Power Ltd, personal communication.
140. H.-W. Chen, K.-C. Huang, C.-Y. Hsu, C.-Y. Lin, J.-G. Chen, C.-P. Lee, L.-Y. Lin, R. Vittal and K.-C. Ho, *Electrochimica Acta*, 2011, 56, 7991-7998.
141. C. H. Lee, W. H. Chiu, K. M. Lee, W. F. Hsieh and J. M. Wu, *Journal of Materials Chemistry*, 2011, 21, 5114-5119.
142. S. Ito, N. L. C. Ha, G. Rothenberger, P. Liska, P. Comte, S. M. Zakeeruddin, P. Péchy, M. K. Nazeeruddin and M. Grätzel, *Chemical Communications*, 2006, DOI: 10.1039/b608279c, 4004-4006.
143. J. Wu, Y. Xiao, Q. Tang, G. Yue, J. Lin, M. Huang, Y. Huang, L. Fan, Z. Lan, S. Yin and T. Sato, *Advanced Materials*, 2012, 24, 1884-1888.

144. J. An, W. Guo and T. Ma, *Small*, 2012, 8, 3427-3431.
145. K. M. Lee, C. Y. Chen, Y. T. Tsai, L. C. Lin and C. G. Wu, *RSC Advances*, 2013, 3, 9994-10000.
146. D. Kuang, J. Brilliet, P. Chen, M. Takata, S. Uchida, H. Miura, K. Sumioka, S. M. Zakeeruddin and M. Graetzel, *ACS nano*, 2008, 2, 1113-1116.
147. T. B. Meyer, A. F. Meyer and D. Ginestoux, *Proc. SPIE*, 2002, 4465, 13-20.
148. R. Kumar, A. K. Sharma, V. S. Parmar, A. C. Watterson, K. G. Chittibabu, J. Kumar and L. A. Samuelson, *Chemistry of Materials*, 2004, 16, 4841-4846.
149. G. Boschloo, H. Lindström, E. Magnusson, A. Holmberg and A. Hagfeldt, *Journal of Photochemistry and Photobiology A: Chemistry*, 2002, 148, 11-15.
150. N. Robertson, *Angewandte Chemie International Edition*, 2006, 45, 2338-2345.
151. T. Miyasaka, *Journal of Physical Chemistry Letters*, 2011, 2, 262-269.
152. F. De Rossi, L. Di Gaspare, A. Reale, A. Di Carlo and T. Brown, *Journal of Materials Chemistry A*, 2013, 1, 12941-12947.
153. D. Garcia-Alonso, V. Zardetto, A. J. M. Mackus, F. De Rossi, M. A. Verheijen, T. M. Brown, W. M. M. Kessels and M. Creatore, *Advanced Energy Materials*, 2014, 4, DOI:10.1002/aenm.201300831.
154. L. Chen, W. Tan, J. Zhang, X. Zhou, X. Zhang and Y. Lin, *Electrochimica Acta*, 2010, 55, 3721-3726.
155. K. Aitola, J. Halme, S. Feldt, P. Lohse, M. Borghei, A. Kaskela, A. G. Nasibulin, E. I. Kauppinen, P. D. Lund, G. Boschloo and A. Hagfeldt, *Electrochimica Acta*, 2013, 111, 206-209.
156. S. G. Hashmi, J. Halme, Y. Ma, T. Saukkonen and P. Lund, *Advanced Materials Interfaces*, 2013, DOI: 10.1002/admi.201300055.
157. K. Yu, Z. Wen, H. Pu, G. Lu, Z. Bo, H. Kim, Y. Qian, E. Andrew, S. Mao and J. Chen, *Journal of Materials Chemistry A*, 2013, 1, 188-193.
158. B. Zhao, H. Huang, P. Jiang, H. Zhao, X. Huang, P. Shen, D. Wu, R. Fu and S. Tan, *The Journal of Physical Chemistry C*, 2011, 115, 22615-22621.
159. J. M. Pringle, V. Armel and D. R. MacFarlane, *Chemical Communications*, 2010, 46, 5367-5369.
160. X. Yin, F. Wu, N. Fu, J. Han, D. Chen, P. Xu, M. He and Y. Lin, *ACS Applied Materials and Interfaces*, 2013, 5, 8423-8429.

161. K.-M. Lee, C.-Y. Hsu, P.-Y. Chen, M. Ikegami, T. Miyasaka and K.-C. Ho, *Physical Chemistry Chemical Physics*, 2009, 11, 3375-3379.
162. Q. Qin, J. Tao and Y. Yang, *Synthetic Metals*, 2010, 160, 1167-1172.
163. M. Wang, A. M. Anghel, B. Marsan, N. L. C. Ha, N. Pootrakulchote, S. M. Zakeeruddin and M. Grätzel, *Journal of the American Chemical Society*, 2009, 131, 15976-15977.
164. J. Burschka, V. Brault, S. Ahmad, L. Breau, M. K. Nazeeruddin, B. Marsan, S. M. Zakeeruddin and M. Grätzel, *Energy & Environmental Science*, 2012, 5, 6089-6097.
165. M. Wu, Q. Zhang, J. Xiao, C. Ma, X. Lin, C. Miao, Y. He, Y. Gao, A. Hagfeldt and T. Ma, *Journal of Materials Chemistry*, 2011, 21, 10761-10766.
166. Q. Jiang, G. Li and X. Gao, *Chem. Commun.*, 2009, 6720-6722.
167. H. Zhou, Y. Shi, D. Qin, J. An, L. Chu, C. Wang, Y. Wang, W. Guo, L. Wang and T. Ma, *Journal of Materials Chemistry A*, 2013, 1, 3932-3937.
168. Y. Wang, M. Wu, X. Lin, Z. Shi, A. Hagfeldt and T. Ma, *Journal of Materials Chemistry*, 2012, 22, 4009-4014.
169. G. Hashmi, K. Miettunen, J. Halme, I. Asghar, H. Vahlman, T. Saukkonen, Z. Huaijin and P. Lund, *Journal of the Electrochemical Society*, 2012, 159, H656-H661.
170. S. Thomas, T. G. Deepak, G. S. Anjusree, T. A. Arun, S. V. Nair and A. S. Nair, *Journal of Materials Chemistry A*, 2014, DOI: 10.1039/c3ta13374e.
171. L.-Y. Lin, C.-P. Lee, R. Vittal and K.-C. Ho, *Journal of Power Sources*, 2010, 195, 4344-4349.
172. P. Hasin, M. A. Alpuche-Aviles, Y. Li and Y. Wu, *The Journal of Physical Chemistry C*, 2009, 113, 7456-7460.
173. Y. Wang, C. Zhao, D. Qin, M. Wu, W. Liu and T. Ma, *Journal of Materials Chemistry*, 2012, 22, 22155-22159.
174. K. Sun, B. Fan and J. Ouyang, *Journal of Physical Chemistry C*, 2010, 114, 4237-4244.
175. S. S. Kim, Y. C. Nah, Y. Y. Noh, J. Jo and D. Y. Kim, *Electrochimica Acta*, 2006, 51, 3814-3819.
176. D. Fu, P. Huang and U. Bach, *Electrochimica Acta*, 2012, 77, 121-127.
177. B. Basol, *Commercialization of High Efficiency Low Cost CIGS Technology Based on Electroplating - Final Technical Progress Report, 28 September 2007 - 30 June 2009*, Report NREL/SR-520-48590, NREL, 2010.
178. G. Syrokostas, A. Siokou, G. Leftheriotis and P. Yianoulis, *Solar Energy Materials and Solar Cells*, 2012, 103, 119-127.

179. F. De Rossi, V. Zardetto, F. Di Giacomo, G. Mincuzzi, A. Reale, A. Di Carlo and T. M. Brown, 2014, manuscript in preparation.
180. Q. Qin and R. Zhang, *Electrochimica Acta*, 2013, 89, 726-731.
181. K. Miettunen, M. Toivola, G. Hashmi, J. Salpakari, I. Asghar and P. Lund, *Carbon*, 2011, 49, 528-532.
182. H. Ellis, N. Vlachopoulos, L. Häggman, C. Perruchot, M. Jouini, G. Boschloo and A. Hagfeldt, *Electrochimica Acta*, 2013, 107, 45-51.
183. Y. Xiao, J. Wu, G. Yue, J. Lin, M. Huang and Z. Lan, *Electrochimica Acta*, 2011, 56, 8545-8550.
184. S. Peng, J. Liang, S. G. Mhaisalkar and S. Ramakrishna, *Journal of Materials Chemistry*, 2012, 22, 5308-5311.
185. T. Muto, M. Ikegami and T. Miyasaka, *Journal of the Electrochemical Society*, 2010, 157, B1195-B1200.
186. S. Ahmad, E. Dell'Orto, J.-H. Yum, F. Kessler, M. K. Nazeeruddin and M. Gratzel, *Chemical Communications*, 2012, 48, 9714-9716.
187. I. Okada and S. Shiratori, *ACS Applied Materials and Interfaces*, 2013, 5, 4144-4149.
188. J. Idigoras, E. Guillen, J. F. Ramos, J. A. Anta, N. Mohammad K and S. Ahmad, *Journal of Materials Chemistry A*, 2013, DOI: 10.1039/c3ta13524a.
189. B. Lee, D. B. Buchholz and R. P. H. Chang, *Energy and Environmental Science*, 2012, 5, 6941-6952.
190. K. H. Hung and H. W. Wang, *Thin Solid Films*, 2013, DOI: 10.1016/j.tsf.2013.10.129.
191. S. Nagarajan, P. Sudhagar, V. Raman, W. Cho, K. S. Dhathathreyan and Y. S. Kang, *Journal of Materials Chemistry A*, 2013, 1, 1048-1054.
192. K.-H. Hung, C.-H. Chan and H.-W. Wang, *Renewable Energy*, 2014, 66, 150-158.
193. K. S. Lee, Y. Lee, J. Y. Lee, J. H. Ahn and J. H. Park, *ChemSusChem*, 2012, 5, 379-382.
194. T. Peng, W. Sun, C. Huang, W. Yu, B. Sebo, Z. Dai, S. Guo and X.-Z. Zhao, *ACS Applied Materials & Interfaces*, 2013, DOI: 10.1021/am404265q.
195. J. M. Kim and S. W. Rhee, *Journal of the Electrochemical Society*, 2012, 159, B6-B11.
196. Y. Fu, Z. Lv, S. Hou, H. Wu, D. Wang, C. Zhang and D. Zou, *Advanced Energy Materials*, 2012, 2, 37-41.
197. C.-M. Chen, C.-H. Chen and T.-C. Wei, *Electrochimica Acta*, 2010, 55, 1687-1695.

198. Y. Xiao, J. Wu, G. Yue, J. Lin, M. Huang, L. Fan and Z. Lan, *Electrochimica Acta*, 2011, 58, 621-627.
199. Y. Xiao, J. Wu, G. Yue, J. Lin, M. Huang, Z. Lan and L. Fan, *Electrochimica Acta*, 2012, 85, 432-437.
200. W. Zeng, G. Fang, X. Wang, Q. Zheng, B. Li, H. Huang, H. Tao, N. Liu, W. Xie, X. Zhao and D. Zou, *Journal of Power Sources*, 2013, 229, 102-111.
201. B. Zhao, H. Huang, P. Jiang, H. Zhao, X. Huang, P. Shen, D. Wu, R. Fu and S. Tan, *Journal of Physical Chemistry C*, 2011, 115, 22615-22621.
202. L. Y. Chang, C. P. Lee, K. C. Huang, Y. C. Wang, M. H. Yeh, J. J. Lin and K. C. Ho, *Journal of Materials Chemistry*, 2012, 22, 3185-3191.
203. Y. Xiao, J. Wu, J. Y. Lin, S. Y. Tai and G. Yue, *Journal of Materials Chemistry A*, 2013, 1, 1289-1295.
204. G. Boschloo and A. Hagfeldt, *Accounts of chemical research*, 2009, 42, 1819-1826.
205. Z. Yu, M. Gorlov, J. Nissfolk, G. Boschloo and L. Kloo, *The Journal of Physical Chemistry C*, 2010, 114, 10612-10620.
206. J.-L. Lan, T.-C. Wei, S.-P. Feng, C.-C. Wan and G. Cao, *The Journal of Physical Chemistry C*, 2012, 116, 25727-25733.
207. H. Wang, J. Bell, J. Desilvestro, M. Bertoz and G. Evans, *Journal of Physical Chemistry C*, 2007, 111, 15125-15131.
208. M. Ikegami, J. Suzuki, K. Teshima, M. Kawaraya and T. Miyasaka, *Solar Energy Materials and Solar Cells*, 2009, 93, 836-839.
209. G. Boschloo, L. Häggman and A. Hagfeldt, *The Journal of Physical Chemistry B*, 2006, 110, 13144-13150.
210. T. Stergiopoulos, E. Rozi, C.-S. Karagianni and P. Falaras, *Nanoscale Research Letters*, 2011, 6, 1-7.
211. C. Zhang, Y. Huang, Z. Huo, S. Chen and S. Dai, *The Journal of Physical Chemistry C*, 2009, 113, 21779-21783.
212. L. Ciammaruchi, S. Penna, A. Reale, T. M. Brown and A. Di Carlo, *Microelectronics Reliability*, 2013, 53, 279-281.
213. R. Harikisun and H. Desilvestro, *Solar Energy*, 2011, 85, 1179-1188.
214. J. H. Kim, H. S. Jung, C. H. Park and T. J. Kang, *Journal of Physics and Chemistry of Solids*, 2014, 75, 31-37.
215. P. Wang, S. M. Zakeeruddin, P. Comte, I. Exnar and M. Grätzel, *Journal of the American Chemical Society*, 2003, 125, 1166-1167.
216. P. Wang, S. M. Zakeeruddin, J. E. Moser, M. K. Nazeeruddin, T. Sekiguchi and M. Grätzel, *Nature Materials*, 2003, 2, 402-407.

217. W. Kubo, S. Kambe, S. Nakade, T. Kitamura, K. Hanabusa, Y. Wada and S. Yanagida, *The Journal of Physical Chemistry B*, 2003, 107, 4374-4381.
218. P. Wang, S. M. Zakeeruddin, P. Comte, I. Exnar and M. Grätzel, *Journal of the American Chemical Society*, 2003, 125, 1166-1167.
219. H.-W. Chen, Y.-D. Chiang, C.-W. Kung, N. Sakai, M. Ikegami, Y. Yamauchi, K. C. W. Wu, T. Miyasaka and K.-C. Ho, *Journal of Power Sources*, 2014, 245, 411-417.
220. M. Marszalek, F. D. Arendse, J.-D. Decoppet, S. S. Babkair, A. A. Ansari, S. S. Habib, M. Wang, S. M. Zakeeruddin and M. Grätzel, *Advanced Energy Materials*, 2013, DOI: 10.1002/aenm.201301235.
221. D. A. Wragg and T. M. Watson, *ECS Transactions*, 2013, 53, 19-28.
222. S. M. Feldt, E. A. Gibson, E. Gabrielsson, L. Sun, G. Boschloo and A. Hagfeldt, *Journal of the American Chemical Society*, 2010, 132, 16714-16724.
223. A. Yella, H.-W. Lee, H. N. Tsao, C. Yi, A. K. Chandiran, M. K. Nazeeruddin, E. W.-G. Diau, C.-Y. Yeh, S. M. Zakeeruddin and M. Grätzel, *Science*, 2011, 334, 629-634.
224. J.-H. Yum, E. Baranoff, F. Kessler, T. Moehl, S. Ahmad, T. Bessho, A. Marchioro, E. Ghadiri, J.-E. Moser and C. Yi, *Nature communications*, 2012, 3, 631.
225. A. Fukui, N. Fuke, R. Komiya, N. Koide, R. Yamanaka, H. Katayama and L. Han, *Applied physics express*, 2009, 2, 082202.
226. S. Dai, K. Wang, J. Weng, Y. Sui, Y. Huang, S. Xiao, S. Chen, L. Hu, F. Kong and X. Pan, *Solar Energy Materials and Solar Cells*, 2005, 85, 447-455.
227. L. Han, A. Fukui, Y. Chiba, A. Islam, R. Komiya, N. Fuke, N. Koide, R. Yamanaka and M. Shimizu, *Applied Physics Letters*, 2009, 94, 013305.
228. A. Hinsch, S. Behrens, M. Berginc, H. Bönemann, H. Brandt, A. Drewitz, F. Einsele, D. Faßler, D. Gerhard and H. Gores, *Progress in Photovoltaics: Research and Applications*, 2008, 16, 489-501.
229. G. E. Tulloch, *Journal of Photochemistry and Photobiology A: Chemistry*, 2004, 164, 209-219.
230. F. Giordano, A. Guidobaldi, E. Petrolati, L. Vesce, R. Riccitelli, A. Reale, T. M. Brown and A. Di Carlo, *Progress in Photovoltaics: Research and Applications*, 2013, 21, 1653-1658.
231. H. Arakawa, T. Yamaguchi, T. Sutou, Y. Koishi, N. Tobe, D. Matsumoto and T. Nagai, *Current Applied Physics*, 2010, 10, S157-S160.
232. A. Kay and M. Grätzel, *Solar Energy Materials and Solar Cells*, 1996, 44, 99-117.

233. F. Matteocci, S. Casaluci, S. Razza, A. Guidobaldi, T. M. Brown, A. Reale and A. Di Carlo, *Journal of Power Sources*, 2014, 246, 361-364.
234. Y. Rong, X. Li, Z. Ku, G. Liu, H. Wang, M. Xu, L. Liu, M. Hu, P. Xiang, Z. Zhou, T. Shu and H. Han, *Solar Energy Materials and Solar Cells*, 2012, 105, 148-152.
235. H.-P. Jen, M.-H. Lin, L.-L. Li, H.-P. Wu, W.-K. Huang, P.-J. Cheng and E. W.-G. Diau, *ACS Applied Materials & Interfaces*, 2013, 5, 10098-10104.
236. K.-M. Lee, C.-Y. Chen, Y.-T. Tsai, L.-C. Lin and C.-G. Wu, *RSC Adv.*, 2013, 3, 9994-10000.
237. Y. Jun, J. Kim and M. G. Kang, *Solar energy materials and solar cells*, 2007, 91, 779-784.
238. Y. Kijitori, M. Ikegami and T. Miyasaka, *Chemistry Letters*, 2007, 36, 190-191.
239. Y. Xiao, J. Wu, G. Yue, J. Lin, M. Huang, L. Fan and Z. Lan, *RSC Advances*, 2012, 2, 10550-10555.
240. F. C. Krebs, *Solar Energy Materials and Solar Cells*, 2009, 93, 465-475.
241. P. Murray, P. Moonie and R. Platts, 2009, WO Patent 2,009,033,214.
242. S. Tulloch, P. Murray, A. Thein, R. Platts, P. Moonie, J. DeSilvestro, G. Tulloch, T. Maine, M. Holding and B. Jausnik, 2009, WO Patent 2,009,033,215.
243. A. Montello, K. Oliver and K. G. Chittibabu, 2010, patent US 7829781
244. A. Montello, K. Oliver and K. G. Chittibabu, 2010, patent US 7777128.
245. A. J. Montello, C. G. Anderson, K. D. Tabor, M. Yalland, M. Bellamy and A. D. Jones, 2009, patent EP2122641.
246. J. Ryan, 2007, patent US7186911.
247. M. Sasaki, 2012, patent US 20120006379.
248. M. I. Asghar, K. Miettunen, J. Halme, P. Vahermaa, M. Toivola, K. Aitola and P. Lund, *Energy & Environmental Science*, 2010, 3, 418-426.
249. M. Grätzel, *Comptes Rendus Chimie*, 2006, 9, 578-583.
250. A. Hinsch, J. Kroon, R. Kern, I. Uhlendorf, J. Holzbock, A. Meyer and J. Ferber, *Progress in Photovoltaics: Research and Applications*, 2001, 9, 425-438.
251. N. Kato, Y. Takeda, K. Higuchi, A. Takeichi, E. Sudo, H. Tanaka, T. Motohiro, T. Sano and T. Toyoda, *Solar Energy Materials and Solar Cells*, 2009, 93, 893-897.
252. P. M. Sommeling, M. Späth, H. Smit, N. Bakker and J. Kroon, *Journal of Photochemistry and Photobiology A: Chemistry*, 2004, 164, 137-144.

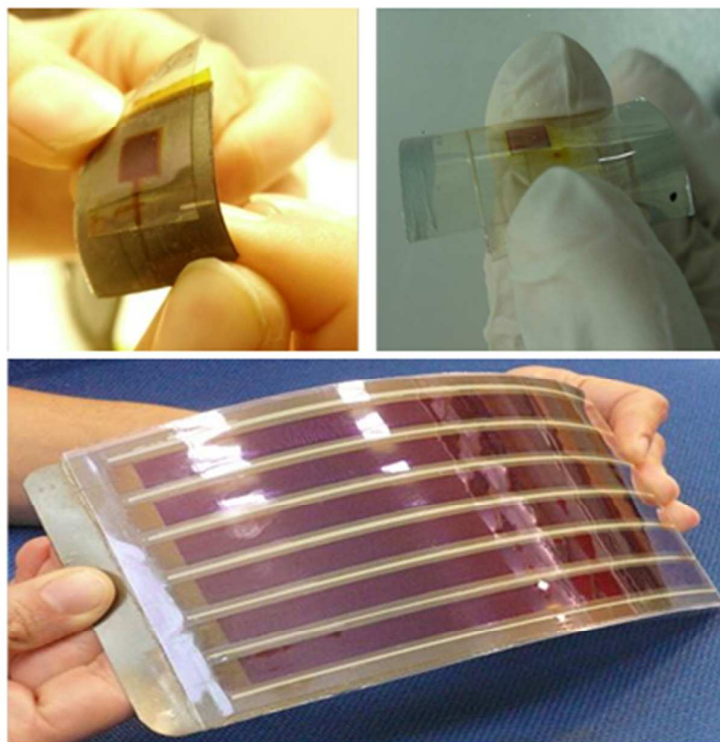
253. S. Ito, M. Nazeeruddin, P. Liska, P. Comte, R. Charvet, P. Péchy, M. Jirousek, A. Kay, S. M. Zakeeruddin and M. Grätzel, *Progress in photovoltaics: research and applications*, 2006, 14, 589-601.
254. J. Kroon, N. Bakker, H. Smit, P. Liska, K. Thampi, P. Wang, S. Zakeeruddin, M. Grätzel, A. Hinsch and S. Hore, *Progress in Photovoltaics: Research and Applications*, 2007, 15, 1-18.
255. P. Wang, C. Klein, R. Humphry-Baker, S. M. Zakeeruddin and M. Grätzel, *Applied Physics Letters*, 2005, 86, 123508.
256. S. Ito, S. M. Zakeeruddin, P. Comte, P. Liska, D. Kuang and M. Grätzel, *Nature Photonics*, 2008, 2, 693-698.
257. R. Y. Ogura, S. Nakane, M. Morooka, M. Orihashi, Y. Suzuki and K. Noda, *Applied Physics Letters*, 2009, 94, 073308.
258. P. Wang, S. M. Zakeeruddin and M. Grätzel, *Journal of Fluorine Chemistry*, 2004, 125, 1241-1245.
259. N. Papageorgiou, *Coordination Chemistry Reviews*, 2004, 248, 1421-1446.
260. M. Ikegami, J. Suzuki, K. Teshima, M. Kawaraya and T. Miyasaka, *Solar Energy Materials and Solar Cells*, 2009, 93, 836-839.
261. J. Scheirs and J.-L. Gardette, *Polymer Degradation and Stability*, 1997, 56, 339-350.
262. S. Mastroianni, M. I. Asghar, K. Miettunen, J. Halme, A. Lanuti, T. M. Brown and P. Lund, *Physical Chemistry Chemical Physics*, 2014, 16, 6092-6100.
263. L.-T. Huang, M.-C. Lin, M.-L. Chang, R.-R. Wang and H.-C. Lin, *Thin Solid Films*, 2009, 517, 4207-4210.
264. C. Law, S. C. Pathirana, X. Li, A. Y. Anderson, P. R. Barnes, A. Listorti and T. H. Ghaddar, *Advanced Materials*, 2010, 22, 4505-4509.
265. K.-M. Lee, S.-J. Wu, C.-Y. Chen, C.-G. Wu, M. Ikegami, K. Miyoshi, T. Miyasaka and K.-C. Ho, *Journal of Materials Chemistry*, 2009, 19, 5009-5015.
266. F. C. Krebs, T. Tromholt and M. Jørgensen, *Nanoscale*, 2010, 2, 873-886.
267. M. Hösel, R. R. Søndergaard, M. Jørgensen and F. C. Krebs, *Advanced Engineering Materials*, 2013, 15, 1068-1075.
268. F. C. Krebs, S. A. Gevorgyan, B. Gholamkhash, S. Holdcroft, C. Schlenker, M. E. Thompson, B. C. Thompson, D. Olson, D. S. Ginley and S. E. Shaheen, *Solar Energy Materials and Solar Cells*, 2009, 93, 1968-1977.
269. S. Cros, R. De Bettignies, S. Berson, S. Bailly, P. Maise, N. Lemaitre and S. Guillerez, *Solar Energy Materials and Solar Cells*, 2011, 95, S65-S69.

270. G. Dennler, C. Lungenschmied, H. Neugebauer, N. Sariciftci, M. Latreche, G. Czeremuszkin and M. Wertheimer, *Thin Solid Films*, 2006, 511, 349-353.
271. L. Fumagalli, M. Binda, I. S. Lopez, D. Natali, M. Sampietro, S. Ferrari, L. Lamagna and M. Fanciulli, *Organic Electronics*, 2009, 10, 692-695.
272. J. Fahlteich, W. Schönberger, M. Fahland and N. Schiller, *Surface and Coatings Technology*, 2011, 205, Supplement 2, S141-S144.
273. J. Wu, Y. Xiao, Q. Tang, G. Yue, J. Lin, M. Huang, Y. Huang, L. Fan, Z. Lan and S. Yin, *Advanced Materials*, 2012, 24, 1884-1888.
274. H. Arakawa, T. Yamaguchi, T. Sutou, Y. Koishi, N. Tobe, D. Matsumoto and T. Nagai, *Current Applied Physics*, 2010, 10, S157-S160.
275. V. Zardetto, G. Mincuzzi, F. De Rossi, F. Di Giacomo, A. Reale, A. Di Carlo and T. Brown, *Applied Energy*, 2014, 113, 1155-1161.
276. D. F. N. Sridhar, presented in part at the 26th European Photovoltaic Solar Energy Conference and Exhibition, 2011.
277. Fujikura, http://www.fujikura.co.jp/eng/f-news/2035577_4207.html.
278. N. Tanabe, Dye-Sensitized Solar Cell for Energy Harvesting Applications, http://www.fujikura.co.jp/eng/rd/gihou/backnumber/pages/_icsFiles/afiel_dfile/2013/05/23/42e_30.pdf.
279. D. F. N. Sridhar, Bringing PV indoors again, http://www.electronicproducts.com/Power_Products/Invertors/Bringing_PV_indoors_again.aspx.
280. SolarPrint, Comparison of Indoor PV modules, [http://www.solarprint.ie/uploads/documents/dssc_am_si_module_comparison\(1\).pdf](http://www.solarprint.ie/uploads/documents/dssc_am_si_module_comparison(1).pdf).
281. D. D'Ercole, L. Dominici, T. M. Brown, F. Michelotti, A. Reale and A. Di Carlo, *Applied Physics Letters*, 2011, 99, 213301.
282. R. Timlin, Understanding the future of smart indoor environments, and how to power them, http://ecosummit.net/uploads/eco12_151112_1300_rorytimlin_solarprint.pdf.
283. <http://www.dyesol.com>.
284. http://www.logitech.com/it-it/home?WT.mc_id=EMEA_DR_IT_Q3_FY14_SERP&WT.srch=1&ci=0&gclid=CP2-8dD9jLwCFcNF3godEAcAJg&utm_medium=cpc&utm_source=g&utm_term=logitech&utm_campaign=digital_river.
285. http://www.argussecurity.it/index.php?option=com_argusnews&id=1.
286. <http://www.skycoshade.com/products.html>.

287. H. Zervos, IDTechEx, Dye Sensitized Solar Cells (DSSC/DSC) 2013-2023: Technologies, Markets, Players, <http://www.idtechex.com/research/reports/dye-sensitized-solar-cells-dssc-dsc-2013-2023-technologies-markets-players-000345.asp?viewopt=showall>.
288. M. B. Schubert and J. H. Werner, *Materials today*, 2006, 9, 42-50.
289. J. Kalowekamo and E. Baker, *Solar Energy*, 2009, 83, 1224-1231.
290. H. S. Jung and J.-K. Lee, *The Journal of Physical Chemistry Letters*, 2013, 4, 1682-1693.
291. T.-Y. Cho, C.-W. Han and S.-G. Yoon, *Journal of Alloys and Compounds*, 2013, 578, 609-612.
292. D. Fu, P. Lay and U. Bach, *Energy & Environmental Science*, 2013, 6, 824-829.
293. S. I. Cha, Y. Kim, K. H. Hwang, Y.-J. Shin, S. H. Seo and D. Y. Lee, *Energy & Environmental Science*, 2012, 5, 6071-6075.
294. X. Fan, Z. Chu, F. Wang, C. Zhang, L. Chen, Y. Tang and D. Zou, *Advanced Materials*, 2008, 20, 592-595.
295. S. Hou, Z. Lv, H. Wu, X. Cai, Z. Chu, Yiliguma and D. Zou, *Journal of Materials Chemistry*, 2012, 22, 6549-6552.
296. S. Hou, X. Cai, H. Wu, Z. Lv, D. Wang, Y. Fu and D. Zou, *Journal of Power Sources*, 2012, 215, 164-169.
297. Y. Fu, M. Peng, Z. Lv, X. Cai, S. Hou, H. Wu, X. Yu, H. Kafafy and D. Zou, *Nano Energy*, 2013, 2, 537-544.
298. Z. Lv, Y. Fu, S. Hou, D. Wang, H. Wu, C. Zhang, Z. Chu and D. Zou, *Physical Chemistry Chemical Physics*, 2011, 13, 10076-10083.
299. H. Sun, X. You, J. Deng, X. Chen, Z. Yang, J. Ren and H. Peng, *Advanced Materials*, 2014, DOI: 10.1002/adma.201305188.
300. D. Angmo and F. C. Krebs, *Journal of Applied Polymer Science*, 2013, 129, 1-14.
301. W. Cai, X. Gong and Y. Cao, *Solar Energy Materials and Solar Cells*, 2010, 94, 114-127.
302. F. C. Krebs, S. A. Gevorgyan and J. Alstrup, *Journal of Materials Chemistry*, 2009, 19, 5442-5451.
303. P. Kumar and S. Chand, *Progress in Photovoltaics: Research and Applications*, 2012, 20, 377-415.
304. G. Li, R. Zhu and Y. Yang, *Nature Photonics*, 2012, 6, 153-161.
305. C. Lungenschmied, G. Dennler, H. Neugebauer, S. N. Sariciftci, M. Glatthaar, T. Meyer and A. Meyer, *Solar Energy Materials and Solar Cells*, 2007, 91, 379-384.

306. A. Mishra and P. Bäuerle, *Angewandte Chemie International Edition*, 2012, 51, 2020-2067.
307. M. Riede, T. Mueller, W. Tress, R. Schueppel and K. Leo, *Nanotechnology*, 2008, 19, 424001.
308. B. Walker, C. Kim and T.-Q. Nguyen, *Chemistry of Materials*, 2010, 23, 470-482.
309. H. Wu, B. Zhao, Z. He, M. Yun, M. Wang, X. Huang, J. Wu and Y. Cao, *Journal of Materials Chemistry C*, 2014, DOI: 10.1039/C3TC32520B.
310. N. Yeh and P. Yeh, *Renewable and Sustainable Energy Reviews*, 2013, 21, 421-431.
311. R. Po, A. Bernardi, A. Calabrese, C. Carbonera, G. Corso and A. Pellegrino, *Energy & Environmental Science*, 2014, 7, 925-943.
312. P. Docampo, J. M. Ball, M. Darwich, G. E. Eperon and H. J. Snaith, *Nature communications*, 2013, 4, 2761.
313. J. You, Z. Hong, Y. Yang, Q. Chen, M. Cai, T.-B. Song, C.-C. Chen, S. Lu, Y. Liu and H. Zhou, *ACS nano*, 2014, 8, 1674-1680.
314. H.-W. Chen, C.-Y. Hsu, J.-G. Chen, K.-M. Lee, C.-C. Wang, K.-C. Huang and K.-C. Ho, *Journal of Power Sources*, 2010, 195, 6225-6231.
315. T. Miyasaka, M. Ikegami and Y. Kijitori, *Journal of the Electrochemical Society*, 2007, 154, A455-A461.
316. S. Wang, J. Zhang, S. Chen, H. Yang, Y. Lin, X. Xiao, X. Zhou and X. Li, *Electrochimica Acta*, 2011, 56, 6184-6188.
317. L. Y. Lin, M. H. Yeh, C. P. Lee, Y. H. Chen, R. Vittal and K. C. Ho, *Electrochimica Acta*, 2011, 57, 270-276.
318. S. Peng, P. Zhu, Y. Wu, S. G. Mhaisalkar and S. Ramakrishna, *RSC Advances*, 2012, 2, 652-657.
319. N. Fu, X. Xiao, X. Zhou, J. Zhang and Y. Lin, *Journal of Physical Chemistry C*, 2012, 116, 2850-2857.
320. X. Yin, Z. Xue and B. Liu, *Journal of Power Sources*, 2011, 196, 2422-2426.
321. J. Usagawa, S. Pandey, Y. Ogomi and S. Hayase, *International Photonics and Optoelectronics Meetings (POEM)*, 2013, DOI:10.1364/AOEE.2013.ASu2C.1.

Table of contents for Manuscript ID TA-FEA-02-2014-000902
Title: Progress in flexible dye solar cell materials, processes and devices



Progress in the development of materials, processes, devices and industrialization of flexible dye solar cells is analyzed in this review.